Bifunctional Charge Transfer Operated Fluorescent Probes with Acceptor and Donor Receptors. 2. Bifunctional Cation Coordination Behavior of Biphenyl-Type Sensor Molecules Incorporating 2,2′:6′,2″-Terpyridine Acceptors

Y. Q. Li,[†,‡] J. L. Bricks,[§] U. Resch-Genger,*[,†] M. Spieles,[†] and W. Rettig[||]

Working Group Optical Spectroscopy, Federal Institute for Materials Research and Testing (BAM), Richard-Willstaetter-Strasse 11, D-12489 Berlin, Germany, National Nanotechnology Laboratory, Lecce University, Distretto Tecnologico, Via Arnesano Km 5, 73100 Lecce, Italy, Institute of Organic Chemistry, National Academy of Sciences of the Ukraine, Murmanskaya 5, 235660 Kiev-94, Ukraine, and Institut für Chemie, Humboldt Universität zu Berlin, Brook-Taylor-Strasse 2, D-12489 Berlin, Germany

Received: March 31, 2006; In Final Form: June 6, 2006

Based on donor (D)−acceptor (A) biphenyl (b) type molecules, a family of fluorescent reporters with integrated acceptor receptors and noncoordinating and coordinating donor substituents of varying strength has been designed for ratiometric emission sensing and multimodal signaling of metal ions and protons. In part 2 of this series on such charge transfer (CT) operated mono- and bifunctional fluorescent devices, the cation coordination behavior of the sensor molecules bpb-R equipped with a proton- and cation-responsive 2,2′:6′,2″-terpyridine (bp) acceptor and either amino-type donor receptors (R = DMA, A15C5 = monoaza-15-crown-5) or nonbinding substituents (R = CF_3, H, OMe) is investigated employing the representative metal ions Na(I), Ca(II), Zn(II), Hg(II), and Cu(II) and steady-state and time-resolved fluorometry. The bpb-R molecules, the spectroscopic behavior and protonation behavior of which have been detailed in part 1 of this series, present rare examples for CT-operated bifunctional fluorescent probes that can undergo consecutive and/or simultaneous analyte recognition. The analyte-mediated change of the probes' intramolecular CT processes yields complexation site- and analyte-specific outputs, i.e., absorption and fluorescence modulations in energy, intensity, and lifetime. As revealed by the photophysical studies of the cation complexes of these fluoroionophores and the comparison to other neutral and charged D−A biphenyls, the spectroscopic properties of the acceptor chelates of bpb-R and A- and D-coordinated bpb-R are governed by CT control of an excited-state barrier toward formation of a forbidden charge transfer state, by the switching between analytically favorable anti-energy and common energy gap law type behavior, and by the electronic nature of the ligated metal ion. This accounts for the astonishingly high fluorescence quantum yields of the acceptor chelates of bpb-R equipped with weak or medium-sized donors and the red emission of D- and A-coordinated bpb-R observed for nonquenching metal ions.

1. Introduction

Molecular devices that undergo strong signal changes as a response to an external chemical trigger are very attractive tools for fluorescence detection and monitoring of nonfluorescent analytes, e.g., either beneficial or harmful metal ions in biology, analytical chemistry, and environmental analysis.[1−4] Suitable fluorescent reporters must efficiently transduce a binding event into a measurable fluorescence signal, thereby taking advantage of the intrinsic selectivity of communication of fluorescence via two experimental parameters, excitation and emission wavelength, and its high sensitivity. A third independent observable is opened by the possibility of signal monitoring in the temporal regime. Such molecular devices are conceived by problem-adapted combination of specific components within a composite design concept to optimize their performance.[5,6] Typically, an auxochrome generating the fluorescence signal is combined with an analyte-responsive receptor via a saturated or unsaturated spacer.[7,8] The sensing properties of such systems depend on the receptor-controlled (chemical) selectivity and the analyte-mediated signaling (spectroscopic) selectivity as well as sensitivity. In (photoinduced) electron transfer (ET) operated probes where the electron systems of fluorophore and binding site are decoupled either by a saturated or a "ZERO-type" spacer in an orthogonal design, the binding event is commonly signaled only by a change in fluorescence quantum yield and lifetime.[7,9,10] In the case of intrinsic probes, both modules chosen to act as donor and acceptor moieties are electronically connected and can undergo an analyte-mediated intramolecular charge transfer (CT) process at least in highly polar media. Accordingly, analyte coordination yields spectral and intensity modulations in absorption and—depending on the binding site involved—also in emission.[8] For donor-type receptors, e.g., nitrogen-containing ligands presenting the typical design concept of this class of sensor molecules, the binding event is communicated via strong changes in absorption but only very moderate changes in emission[11] due to the release or decoordination of the metal ion upon electronic excitation of the complexed probe.[12] Prevention of the latter is the prerequisite for analytically favorable ratiometric emission signaling that provides an increase in dynamic range and a built-in correction

[†] BAM.
[‡] Lecce University.
[§] National Academy of Sciences of the Ukraine.
[||] Humboldt Universität zu Berlin.

10.1021/jp062013q CCC: $33.50
Published on Web 09/02/2006

for environmental effects via signal ratioing. Realization of strong coordination-induced spectral changes also in emission requires rational tuning of the probe's donor (D)−acceptor (A) strength for D-type receptors[13] as, e.g., is demonstrated in part 3 of this series on bifunctional CT-operated fluoroionophores,[14] the use of acceptor-type binding sites,[15,16] participation of the electron-accepting chromophore in analyte coordination,[17] D−D substituted sensor molecules,[18,19] or the combination of two CT processes in a more complex D^1-A-D^2 type design.[20,21] Alternative strategies toward ratiometric sensing, which are beyond the scope of this article, are molecules equipped either with two chromophores[22−24] or with a fluorophore, the emission spectrum of which is extremely sensitive to the polarity of the local environment[25] as well as chemodosimeters.[26]

Aside from ongoing research efforts dedicated to the development of improved sensor molecules for metal ions, anions, and organic molecules,[1,7,8,27] other even more challenging research activities in chemical sensing focus on advanced sensory devices that can, for instance, simultaneously or cooperatively report different inputs or a single analyte over an extended dynamic range.[28] Potential applications of such sophisticated fluorescent reporters could eventually be, e.g., the monitoring of bidirectional ion fluxes or of the presence of competing metal ions at the same location within a cell. Rationalization of such devices requires the proper choice and combination of more than two functional components, i.e., receptor and/or reporter units.[6,29−31] A straightforward approach is bifunctional fluorescent probes equipped with two receptors that vary either in cation selectivity or in the complexation/protonation constant and generate coordination-site-specific, spectroscopically clearly distinguishable signals, e.g., strong alterations in intensity and/or energy as well as fluorescence lifetime depending on the underlying operation principle.[21,29] This provides the basis for the communication of whether *none*, *only one*, *the other*, or *both* binding sites are involved in analyte coordination as typically desired for multimodal sensing of two different chemical inputs. For bifunctional probes that display an extended dynamic range for a single analyte upon consecutive coordination of both receptors, this sensing scheme corresponds to different concentration regimes, e.g., *none*, *little* (below a certain threshold; one receptor bound), and *much* (above a certain threshold; both receptors engaged).[32,33] At present, the majority of bifunctional molecules as well as fluorescent devices with logic action respond to combinations of protons and alkali or alkaline earth metal ions and are ET-operated, i.e., limited to intensity alterations.[29,34] Up to now, there have been only a few examples reported for bifunctional CT-operated molecules as well as for systems signaling transition metal ions.[19,21,21,34−37]

In this paper on CT-operated ratiometric and bifunctional devices, we focus on the cation coordination behavior of D−A biphenyl-type molecules bpb-R with integrated electron-accepting 2,2′:6′,2″-terpyridine receptors and various noncoordinating (R = CF_3, H, OMe) and coordinating (R = DMA (dimethylamino), A15C5) substituents R of different donor strength (see Scheme 1) as an extension of our studies on the spectroscopic properties and protonation behavior of bpb-R revealed in part 1 of this series.[38] The goal of part 2 is to derive structure−property relationships for CT-operated sensor molecules that (i) enable ratiometric emission sensing of nonquenching and quenching metal ions[39] and (ii) can exist in three or four spectroscopically distinguishable states when equipped with two properly chosen coordination sites. The latter implies communication of whether the sensor molecule is in the *analyte-free*, *A-coordinated*, *D-coordinated*, or *A- and D-coordinated* state.

SCHEME 1: Chemical Structures of bpb-R with R = CF_3 (1), H (2), OMe (3), DMA (4), and A15C5 (5)

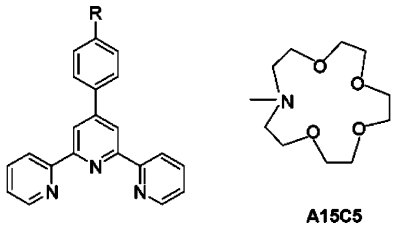

A15C5

SCHEME 2: Chemical Structures of Related Neutral and Ionic D−A Biphenyls 6, 6a, 7, and 8, with R = H, OMe, and DMA, and Bifunctional D−D Biphenyl Sensor Molecule 9

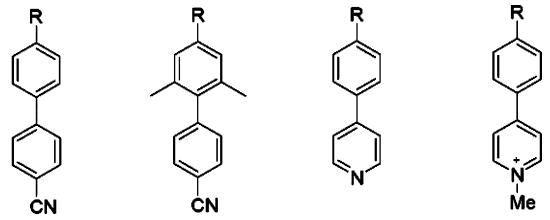

6 **6a** **7** **8**

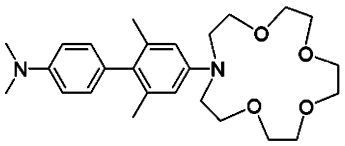

9

The bpb-R fluorescent reporters are designed to combine the well-described complexation properties of terpyridines, tridentate electron-accepting ligands,[40−44] with the D−A strength-controlled spectroscopic features of D−A substituted biphenyls.[45−50] Some biphenyls such as molecule **6a**[45] (see Scheme 2), show comparatively high fluorescence quantum yields of a twisted intramolecular charge transfer (TICT) like emission[51,52] and an analytically favorable anti-energy gap law type behavior.[38] To provide the basis for bifunctional sensing of bpb-R from the receptor chemistry, we chose a dimethylamino and a monoaza crown donor subsituent because the basicity, cation selectivity, and complexation constants of these D-receptors are expected to strongly differ from the corresponding properties of the terpyridine acceptor. Strong differences in the cation selectivity and basicity of both ligating sites are the chemical prerequisite for the simultaneous recognition of two chemical inputs, either two different metal ions or a metal ion and protons, whereas sufficient differences in binding constants are mandatory for consecutive sensing of a single analyte over an extended dynamic range.[21,32,37] The bpb-R series is not designed for real-world analytical applications that typically require operation in aqueous systems, chromophores emitting in the visible/near-infrared spectral region, and very selective ligands, but is designed for the systematic investigation of acceptor vs donor coordination and the evaluation of design principles for ratiometric and bimodal sensing. Accordingly, comparison with other spectroscopically well-characterized model systems is desired, the majority of which have been investigated in acetonitrile.

In a first step, the spectroscopic properties of the acceptor chelates of bpb-R with the representative nonquenching and quenching metal ions Na(I), Ca(II), Zn(II), Hg(II), and Cu(II) are studied and the observed effects are compared to protonation-mediated effects detailed in part 1 of this series.[38] In a second step, the potential of bpb-A15C5 and bpb-DMA for the simultaneous recognition of selected pairs of analytes is illustrated as well as their suitability for sensing of a single analyte over an extended dynamic range. The spectroscopic features of the A- and D-chelates of bpb-R and of A- and D-coordinated bpb-R are discussed within the framework of related D−A substituted neutral and ionic biphenyls and 4′-aryl-substituted pyridines, such as **6**, **6a**, **7**, and **8** shown in Scheme 2, and are compared to the properties of the complexes of D−D biphenyl **9**.[19] As an extension of the chemosensor studies, we investigate the ability of bpb-DMA and bpb-A15C5 to perform logic operations with metal ions and protons.

2. Experimental Section

2.1. Materials. All the chemicals used for the synthesis of the fluorescent probes were purchased from Merck. The metal ion perchlorates purchased from ALFA were of the highest purity commercially available and were dried in a vacuum oven before use.[53] All the solvents employed were of spectroscopic grade and purchased from Aldrich. Prior to use, all the solvents were checked for fluorescent impurities.

2.2. Apparatus. The chemical structures of the synthesized compounds were confirmed by elemental analysis, ^{1}H NMR, and ^{13}C NMR. Their purity was checked by fluorescence spectroscopy. Melting points (uncorrected) were measured with an IA 9100 digital melting point analyzer (Kleinfeld GmbH), and NMR spectra were obtained with a 500 MHz NMR spectrometer, Varian Unity$_{plus}$ 500.

Elemental analyses were performed in duplicate and were carried out at the Institute of Organic Chemistry, National Academy of Sciences of the Ukraine, Kiev, with samples dried prior to analysis for 5−6 h at 80 °C in vacuo following routine procedures.

2.3. Steady-State Absorption and Fluorescence. The UV/vis spectra were recorded on a Carl Zeiss Specord M400/M500 and a Bruins Instruments Omega 10 absorption spectrometer. The fluorescence spectra were measured with a Spectronics Instruments 8100 and a Perkin-Elmer LS 50B spectrofluorometer. Unless otherwise stated, all the fluorescence spectra presented are corrected for the wavelength- and polarization-dependent spectral responsivity of the detection system traceable to the spectral radiance scale. This instrument-specific quantity was determined with a calibrated quartz halogen lamp placed inside an integrating sphere and a white standard, both from Gigahertz-Optik GmbH in the case of the 8100 fluorometer and with spectral fluorescence standards with known corrected emission spectra for the LS50B fluorometer following previously described procedures.[54,55] The emission spectra on a wavenumber scale were obtained by multiplying the measured and corrected emission spectra with λ^2.[56] The absorption and emission maxima given are determined from the respective spectra plotted on an energy scale.

The fluorescence quantum yields (ϕ_f), which were measured with the 8100 fluorometer with Glan Thompson polarizers placed in the excitation channel and the emission channel set to 0° and 54.7°, were calculated from integrated, blank, and spectrally corrected emission spectra (wavelength scale; prior to integration multiplication with λ)[55] employing quinine sulfate in 1 N H_2SO_4 ($\phi_f = 0.55 \pm 0.03$)[57] and coumarin 153 in ethanol ($\phi_f = 0.4$)[58] as fluorescence standards. For each compound−solvent pair, the quantum yield was determined twice. Typical uncertainties of fluorescence quantum yield measurements as derived from previous measurements are ±5% (for $\phi_f > 0.4$), ±10% (for $0.2 > \phi_f > 0.02$), ±20% (for $0.02 > \phi_f > 0.005$), and ±30% (for $0.005 > \phi_f$), respectively.[36]

2.4. Time-Resolved Fluorescence. Fluorescence decay curves were recorded with the time-correlated single-photon-counting technique (TCSPC)[59] using an Ar ion pumped Ti:sapphire laser as excitation source and a previously described setup[60] as well as with a similar setup at the Berlin Synchrotron facility BESSY II. The latter employs synchrotron radiation as excitation light source in conjunction with an excitation monochromator (Jobin Yvon, II, 10 UV). BESSY II delivers a 1.25 MHz pulse train with characteristic pulse widths of 30−50 ps. The fluorescence decays were detected with a microchannel plate photomultiplier tube (MCP; Hamamatsu R 1564-U-01) cooled to −30 °C that was coupled to an emission monochromator (Jobin Yvon II, 10 VIR) by means of quartz fiber optics. The signal from a constant fraction discriminator (CFD; Tennelec 454) was used as the start pulse for the time-to-amplitude converter (TAC; Tennelec TC864) operated in the reverse mode. The BESSY II synchronization pulse was applied as the stop pulse. The MCP pulses were amplified by an amplifier (INA 10386) and coupled into the CFD. A multichannel analyzer (Fast Comtec MCDLAP) was employed for data accumulation. The decays were analyzed by the least-squares iterative reconvolution method on the basis of the Marquardt−Levenberg algorithm, which is implemented into the commercial global analysis program.[61] The instrument response function (IRF), which was obtained by the detection of Rayleigh scattered light in a scattering solution, had a width of 50−60 ps for the laser setup used and a width of 120 ps in the case of the experiments at BESSY II. The quality of the exponential fits was evaluated on the basis of the reduced χ^2 values.

2.5. Synthesis. The bpb-R series was prepared following literature procedures with the synthesis of bpb-H, bpb-OMe, and bpb-DMA having been previously described[62−64] and the synthesis of bpb-CF_3 and bpb-A15C5 having been reported by us.[38]

3. Results and Discussion

To conceive the potential of the bpb-R molecules **1**−**5** as ratiometric fluorescent reporters for metal ions (see Scheme 1), the spectroscopic properties of their acceptor chelates with the representative nonquenching and quenching metal ions Na(I), Ca(II), Zn(II), Hg(II), and Cu(II) are investigated in acetonitrile employing steady-state and time-resolved fluorometry. These metal ions were chosen according to the following criteria: Na(I) and Ca(II) are supposed to bind exclusively to the donor receptor A15C5, whereas the nonquenching transition metal ion Zn(II) and the classical fluorescence quenchers Cu(II) and Hg(II)[39] are expected to preferably coordinate to the terpyridine acceptor moiety. To derive structure−property relationships for biphenyl-type ratiometric sensor molecules for metal ions, the spectroscopic properties of the acceptor chelates of bpb-R are compared with respect to (i) the CT character of the complexes that reveals both the donor strength of R and the strength of the cation−terpyridine interactions and (ii) the cation's electronic nature. Accordingly, a comparison between cation coordination induced and recently presented protonation-induced spectroscopic features of bpb-R[38] is performed, focusing on the acceptor chelates of nonquenching Zn(II). The observed effects are compared to the properties of monocoordinated **9**[19] and are

TABLE 1: Spectroscopic Properties of the Complexes of bpb-R with Selected Metal Ions in Acetonitrile at Room Temperature

compound	$\nu_{abs}{}^a \times 10^3/cm^{-1}$	$\nu_{em}{}^b \times 10^3/cm^{-1}$	$\Delta\nu_{St}{}^c \times 10^3/cm^{-1}$	$\Delta\nu_{fp-cp}{}^d \times 10^3/cm^{-1}$	$\phi_f{}^e$
1	31.8	27.8	4.0		0.24
1⊂Zn^{2+}	29.5	28.2	1.3	2.3, −0.4	0.58
1⊂Hg^{2+}	29.4	n.d.[f]	n.d.	2.4, n.d.	n.d.
1⊂H^+	30.2	25.6	4.6	1.6, 2.2	0.27
prot **1**	30.6	28.0	2.6	1.2, −0.2	0.69
2	32.2	29.2, 28.4	3.0		0.14
2⊂Zn^{2+}	29.7	27.6	2.1	2.5, 1.6	0.52
2⊂Ca^{2+}	30.1	27.7	2.4	2.1, 1.5	0.47
2⊂Cu^{2+}	29.1	n.d.	n.d.	3.1, n.d.	n.d.
2⊂Hg^{2+}	30.9	27.1	3.8	1.3, 2.1	4×10^{-3}
2⊂H^+	30.6	25.5	5.1	1.6, 3.7	0.28
2⊂$2H^+$	30.8	22.0	8.8	1.4, 7.2	0.32
3	35.1, 32.2(sh)	26.0	6.2		0.17
3⊂Zn^{2+}	29.7	21.7	8.0	2.5, 4.3	0.39
3⊂Ca^{2+}	31.6	22.8	8.8	0.6, 3.2	0.58
3⊂Cu^{2+}	28.9	21.7	7.2	3.3, 4.3	4×10^{-4}
3⊂Hg^{2+}	30.1	21.2	8.9	2.1, 4.8	0.02
3⊂H^+	29.7	20.2	9.5	2.5, 5.8	0.07
3⊂$2H^+$	31.5	17.0	14.5	0.7, 9.0	4×10^{-3}
4	29.2	19.4	9.8		0.15
4⊂Zn^{2+}	23.6	16.0	7.6	5.6, 3.4	7×10^{-4}
4⊂Ca^{2+}	25.1	16.7	8.4	4.1, 2.7	6×10^{-3}
4⊂Cu^{2+}	22.9	n.d.	n.d.	6.3, n.d.	n.d.
Cu^{2+}⊃**4**⊂Cu^{2+}	30.4	21.1	9.3	−1.2, −1.7	n.d.
H^+⊃**4**⊂Cu^{2+}	30.0, 29.0(sh)	25.3	3.7	0.2, −5.9	n.d.
4⊂Hg^{2+}	23.7	15.9	7.8	5.5, 3.5	5×10^{-4}
4⊂xH^+[g]	21.4	n.d.	n.d.	7.8, n.d.	n.d.
H^+⊃4⊂xH^+	30.3	28.1	2.2	−1.1, −8.7	0.43
5	28.6	19.9	8.7		0.18
5⊂Zn^{2+}	23.4	16.2	7.2	5.2, 3.7	3×10^{-3}
5⊂Ca^{2+}[h]	25.6	16.9	8.7	3.0, 3.0	0.03
Ca^{2+}⊃**5**⊂Ca^{2+}[i]	30.9	17.7	13.2	−2.3, 2.2	0.10
Na^+⊃**5**	30.9	19.0	11.9	−2.3, 0.9	0.15
Na^+⊃**5**⊂Zn^{2+}	31.3	17.1	7.3	−2.7, 2.8	n.d.

[a] Lowest energy absorption band. [b] Emission maximum. [c] Stokes shift, i.e., energetic difference between the longest wavelength absorption band (or shoulder) and the emission maximum. [d] Coordination-induced spectral shift in absorption (first value) and emission (second value) between free probe and complexed or protonated probe with "fp" and "cp" equaling free probe and coordinated probe. [e] Fluorescence quantum yield. [f] n.d., not determined. [g] Only spectroscopic discrimination between A- and D-protonation and A-protonation of **4** was possible. [h] Metal ion to ligand concentration ratios M:L ≤ 10:1. [i] Metal ion to ligand concentration ratios M:L ≥ 1000:1. bpb-R⊂M^{n+} denotes acceptor chelate, M^{n+}⊃bpb-R denotes donor chelate, and M^{n+}⊃bpb-R⊂M^{n+} denotes D- and A-coordinated probe.

discussed within the framework of neutral and ionic biphenyls, examples of which are depicted in Scheme 2.

3.1. Acceptor Coordination of bpb-R. As follows from Table 1 summarizing the spectroscopic properties of the cation complexes of **1**−**5**, the bpb-R sensor molecules undergo sizable red shifts in absorption and emission not only with Zn(II), Hg(II), and Cu(II), but also with Ca(II). These effects clearly indicate acceptor chelation. The astonishing formation of a strong Ca(II) terpyridine complex in acetonitrile that contradicts our assumption on the cation selectivity of bpb-R and literature data on the complexation properties of terpyridine ligands[40,65] is tentatively ascribed to the poor solvation of the calcium perchlorate in this solvent as compared to water. Only Na(I) does not interact with the terpyridine moiety, as suggested by the lack of spectroscopically detectable effects.

Stoichiometry of the Acceptor Chelates. In aqueous solution, terpyridine ligands typically form 1:2 complexes (M:L, with metal ion M and ligand L) with many metal ions.[40,65] However, the different selectivity of bpb-R compared to that of terpyridines reported in the literature encouraged us to investigate the stoichiometry of the acceptor chelates of bpb-R in acetonitrile exemplary for **2** and **3** with Ca(II), Zn(II), Hg(II), and Cu(II) according to the method of continuous variation.[66] Figure 1 presents the typical result for a continuous variation diagram where the difference Y between the measured absorbance E and the calculated absorbance E' is plotted vs the molar fraction x_L ($x_L = c_L/(c_M + c_L)$, where c_M and c_L refer to the concentrations of ligand and metal ion). As follows from Figure 1, for **3** and Zn(II), maxima at $x_L = 0.66$ are found for 284, 328, and 341

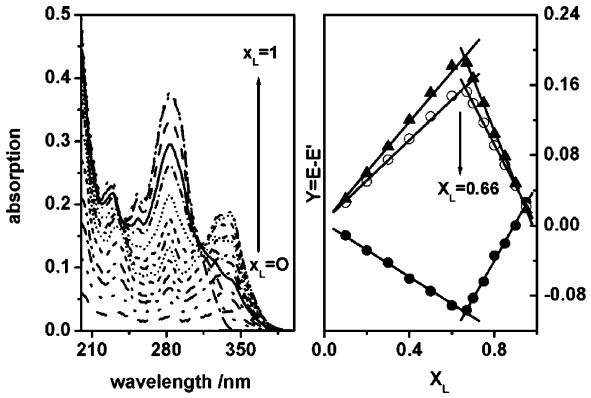

Figure 1. Determination of the complex stoichiometry for bpb-R with R = OMe (**3**) and Zn(II) using the method of continuous variations. Left: Absorption spectra of mixtures of **3** and Zn(II) varying in the molar fraction (x_L) of the ligand (L). Right: Absorbance (E) plot typical for the method of continuous variation for selected wavelengths, i.e., 284 nm (filled circles), 328 nm (open circles), and 341 nm (filled triangles). $x_L = c_L/(c_M + c_L)$, where c_L and c_M are the concentrations of the ligand and the metal ion employed. $Y = E - E'$, where E is the measured absorbance and E' is the calculated absorbance at a selected wavelength. These data are representative for all the other cation complexes of the bpb-R series.

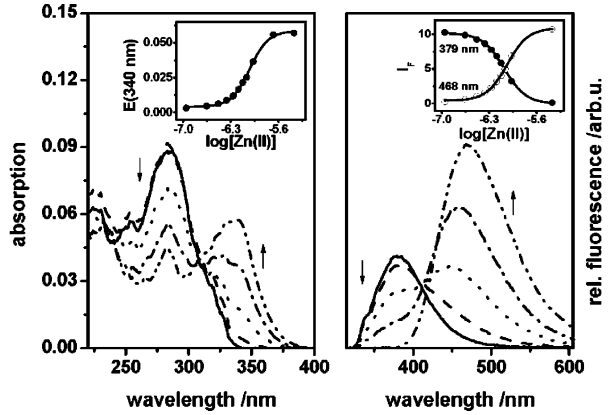

Figure 2. Complexation-induced changes in absorption (left) and emission (right) for bpb-R with R = OMe (**3**) and Zn(II) in acetonitrile for selected metal ion to ligand (M:L) concentration ratios: 0:1 (solid line), 0.1:1 (dashed line), 0.3:1 (dotted line), 0.5:1 (dash−dotted line), and 2:1 (dash−dot−dotted line). The probe concentration was 2×10^{-6} M, and excitation was at 310 nm at the isosbestic point. Insets: Absorption (left; 340 nm) and fluorescence intensity (right; 379 nm: full circles, 468 nm: open circles) as a function of zinc concentration for selected wavelengths.

nm, respectively, indicating the formation of a 2:1 metal ion to ligand complex as the single species. Similar complex stoichiometries were found for all the other acceptor chelates.

To reveal the acceptor coordination-induced changes in absorption and emission of bpb-R, the titration of **3** with zinc is depicted in Figure 2 as an example. Formation of the zinc acceptor chelate is accompanied by the disappearance of the longest wavelength absorption band of the ligand at 286 nm and the appearance of a new red shifted absorption band of CT nature located at ca. 340 nm. Simultaneously, the emission band is bathochromically shifted from 389 to 470 nm. The concentration dependences of these effects are displayed in the insets in Figure 2. These analytically favorable spectral changes reflect the chelation-induced increase in acceptor strength and thus CT character of **3**. The clear course of cation complexation follows from the observation of an isosbestic point at ca. 310 nm (see Figure 2) and from the result of the stoichiometry studies. The comparatively weak chelation-induced changes of the spectral position and vibrational structure of the terpyridine-localized intraligand absorption transitions at wavelengths below ca. 280 nm are not further evaluated. No attempts are made by us to determine the corresponding complexation constants as the small metal ion to ligand concentration ratios required for complete acceptor complexation suggest high complexation constants, the determination of which is rather uncertain with optical methods.

Influence of the Probes' CT Character on Acceptor Chelation. In a second step, the spectroscopic effects accompanying bpb-R coordination are studied as a function of the CT character of the fluorescent probe and the electronic nature of the bound metal ion. Special emphasis is dedicated to the size of the chelation-induced spectral shifts that reveals the strength of the terpyridine-metal ion interactions and to the changes in fluorescence intensity, i.e., quantum yield. A comparison of the absorption properties and the quantum yield-weighted emission spectra of the cation complexes of bpb-R is shown representatively for **3** in Figure 3. As follows from this figure and from Table 1, which summarizes the spectroscopic data of the other cation complexes of bpb-R, the spectral positions of both the acceptor chelate's lowest energy absorption band of CT nature and its emission band clearly depend on the cation bound. The strongest effects occur for Cu(II) in absorption and for Hg(II) in emission. Contrary to typical CT-operated probes with donor

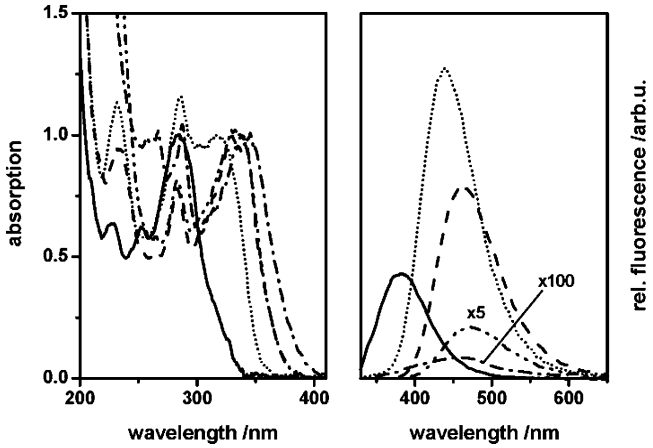

Figure 3. Normalized absorption (left) and quantum yield weighted corrected emission (right) spectra of bpb-R with R = OMe (**3**) (solid line) and its complexes with Zn(II) (dashed line), Ca(II) (short dotted line), Cu(II) (dash−dotted line), and Hg(II) (dash−dot−dotted line). The quantum yield of the free ligand was set to 1. The ligand concentration was 2×10^{-6} M, and the solvent was ACN. Excitation was at 286 nm for **3** and at the maximum of the lowest energy absorption band for the cation complexes.

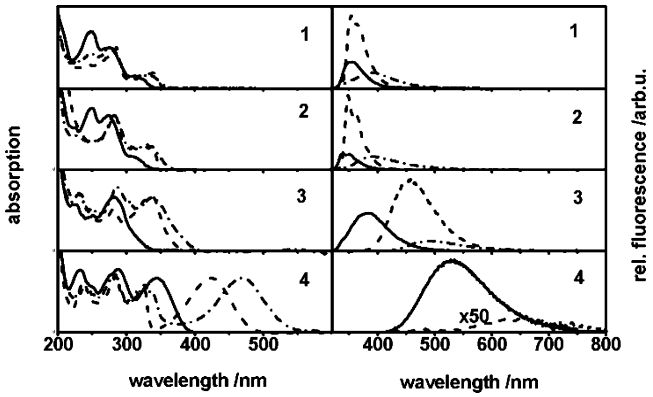

Figure 4. Complexation-induced effects in absorption (left) and emission (right) for bpb-R **1**−**4** (see Scheme 1) and zinc and comparison to monoprotonation-induced effects: L equaling bpb-R (solid line), $L \subset Zn^{2+}$ (dashed line), and monoprotonated $L \subset H^{+}$ (dash−dotted line) in ACN with $L \subset M^{n+}$ symbolizing the acceptor chelate, i.e., the A-coordinated probe. For better visualization of the coordination-induced effects on the probe's fluorescence quantum yield, the corrected emission spectra of the zinc complexes and monoprotonated species are weighted by relative quantum yields with the quantum yield of the ligand equaling 1. Monoprotonated **4** is nonemissive.

coordination reported in the literature, the complexation-induced shifts in emission are strong and even exceed those in absorption for A-coordinated **3**. As to be expected for our design concept, cation binding seems to be enhanced in the excited state due to the excitation-induced increase in electron density at the acceptor site. For a better understanding of the chelation-induced spectral and intensity changes in absorption and emission, we compared the cation coordination induced and (mono)protonation-induced effects in Figure 4 employing zinc A-chelates as model systems for acceptor chelation. As revealed by Figure 4 and Table 1, in most cases the size of the monoprotonation-induced spectral changes in absorption is smaller than that of the corresponding complexation-induced effects. In emission, this trend is reversed. This comparison also illustrates the influence of the substituent R on the spectroscopic features of the resulting acceptor chelates with the size of the chelation-induced shifts in absorption and emission clearly depending on the donor strength of R for a given analyte.

TABLE 2: Fluorescence Lifetimes, Radiative Rate Constants, and Nonradiative Rate Constants of the Cation Complexes of bpb-R

compound	ϕ_f[a]	τ_f[b]/ns	k_f[c]/10^7 s^{-1}	k_{nr}[d]/10^7 s^{-1}
1	0.24	2.1	11	36
1⊂Zn^{2+}	0.58	2.6	22	16
1⊂H^+	0.27	2.5	11	29
prot **1**	0.69	2.7	26	11
2	0.14	1.2	12	72
2⊂Zn^{2+}	0.52	2.6	20	19
2⊂Hg^{2+}	4×10^{-3}	2.7	0.2	37
2⊂H^+	0.28	7.0	4	10
2⊂$2H^+$	0.32	7.4	4	9
3	0.17	2.1	8	40
3⊂Zn^{2+}	0.39	4.1	10	15
3⊂Hg^{2+}	0.02	3.6	0.6	27
3⊂H^+	0.07	1.8	4	52
3⊂$2H^+$	4×10^{-3}	0.3	1	332
4	0.15	5.6	3	15
4⊂Zn^{2+}	7×10^{-4}	0.1	0.7	n.d.
4⊂Hg^{2+}	5×10^{-4}	<55 ps	4	n.d.
H^+⊃**4**⊂xH^+	0.43	1.9	23	30
5	0.18	5.7	3	14
5⊂Zn^{2+}	3×10^{-3}	0.2	2	499
5⊂Ca^{2+}[e]	0.03	0.7	4	139
Ca^{2+}⊃**5**⊂Ca^{2+}[f]	0.10	2.0	5	45
Na^+⊃**5**	0.15	4.5	3	19

[a] Fluorescence quantum yield. [b] Fluorescence lifetime. [c] Radiative rate constant $k_f = \phi_f/\tau_f$. [d] Nonradiative rate constant $k_{nr} = (1 - \phi_f)/\tau_f$. [e] Metal ion to ligand concentration ratios M:L ≤ 10:1. [f] Metal ion to ligand concentration ratios M:L ≥ 1000:1.

Fluorescence Quantum Yields of the Acceptor Chelates of bpb-R. As displayed in Table 1, Figure 3, and Figure 4, a chelation-induced enhancement in fluorescence quantum yield and a strongly emissive character of the acceptor chelates are only observed for the nonquenching metal ions Ca(II) and Zn(II) and for the fluorescent reporters **1**−**3** with a small or medium CT character. As follows from Table 1, the fluorescence quantum yields of the Zn(II) complexes of **3**, **4**, and **5** with their red shifted emission bands are reduced compared to the Ca(II) chelates. For **2**, this trend is reversed. The acceptor chelates of **4** and **5** equipped with strong donors are generally only weakly emissive (see Table 1), with the fluorescence quantum yields of the A-chelates of **5** exceeding those of the respective complexes of **4** that emit at slightly longer wavelengths typically by a factor of ca. 5. Astonishingly, the Ca(II) acceptor chelate of **5**, **5**⊂Ca^{2+}, still displays a moderate fluorescence quantum yield of 0.03 despite its strongly red shifted emission band. For the classical quenchers Cu(II) and Hg(II), the emission of A-coordinated bpb-R is always at least strongly diminished or even completely quenched; see Table 1.

Fluorescence Lifetimes, Radiative Rate Constants, and Nonradiative Rate Constants of the Acceptor Chelates. For a better understanding of the photophysical processes governing the relaxation of the fluorescence of the cation complexes of bpb-R, we investigated the fluorescence decay kinetics of representative complexes at several emission wavelengths within the respective emission bands, focusing on nonquenching Zn(II) and quenching Hg(II). In all cases, the time-resolved-fluorescence measurements display monoexponential decay kinetics with the corresponding lifetimes collected in Table 2. For comparative purposes, the spectroscopic properties of the protonated ligands discussed in part 1 of this series[38] are also included in this table. The most striking observations are the increased fluorescence lifetimes as well as the comparatively high radiative rate constants and small k_{nr} values of the zinc A-chelates of **1**−**3** and the strong reduction of the radiative rate constants and the strong increase of the nonradiative rate constants of the acceptor chelates for **4** and **5**. For example, the k_f values of the zinc acceptor chelates of **1** and **2** exceed those of the parent sensor molecules by a factor of ca. 2. Simultaneously, the nonradiative rate constants are reduced by a factor of ca. 2−4. The k_f values of the zinc complexes of **1**−**3** also exceed those of monoprotonated **1**, **2**, and **3**. The mercury complexes of bpb-R always show very low k_f values. In the cases of **2** and **3**, they display increased fluorescence lifetimes and decreased k_{nr} values with respect to the uncomplexed probes, similar to the corresponding zinc complexes.

3.2. Donor Coordination of bpb-R. Exclusive donor coordination can only be achieved with **5** and Na(I) leading to the characteristic hypsochromic and hyperchromic shifts of the absorption spectra of the complex, thereby reflecting the reduction of the probe's CT character and conjugation length; see Table 1. As often observed for donor coordination of such a CT-operated probe, the spectral position of the emission band remains unaffected.[8,12] The fluorescence quantum yield is more or less unaffected and only a small change in fluorescence lifetime occurs; see Table 2. The complexation constant (log $K_s = 2.6$) determined for Na^+⊃**5** from absorption measurements assuming a 1:1 stoichiometry for the donor chelate is comparable in size to binding constants reported for related literature systems and Na(I).

3.3. Acceptor and Donor Coordination of bpb-R. Among the bpb-R family, only bpb-DMA and bpb-A15C5 are designed for simultaneous or successive acceptor and donor coordination of two different analytes or a single species at different concentration regimes. For these bifunctional complexation studies, it must be kept in mind that, due to the 1:2 stoichiometry of the acceptor chelates, the situation can be further complicated for donor coordination by the intermediate formation of mixed complexes with one donor substituent R of the two A-coordinated ligands being coordinated to the analyte and the other one being uncomplexed followed by complete donor coordination eventually. Also, the two acceptor-bound sensor molecules may electronically interact, and consequently, their subsequent donor coordination may not be independent of each

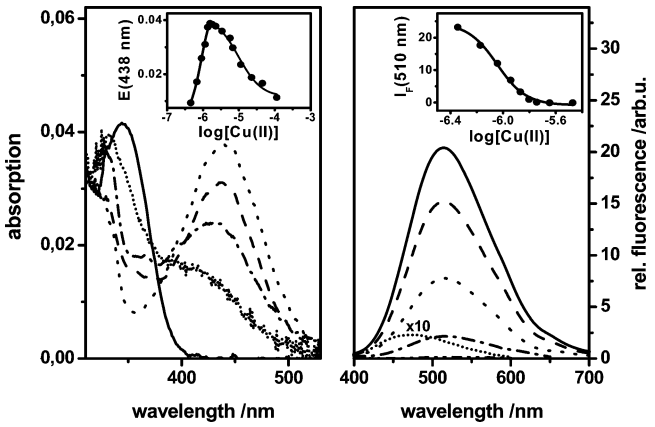

Figure 5. Absorption (left) and fluorescence (right) spectra of bpb-R with R = DMA (**4**) as a function of Cu(II) concentration. The copper ion to ligand concentration ratios were 0:1 (solid line), 0.5:1 (dashed line), 1:1 (dotted line), 5:1 (dash−dotted line) and 50:1 (short dotted line) for absorption and 0:1 (solid line), 0.2:1 (dashed line), 0.4:1 (dotted line), 0.6:1 (dash−dotted line), 0.8:1 (dash−dot−dotted line) and 5:1 (short dotted line; multiplied by a factor of 10) for emission. Different Cu(II):L ratios were chosen for absorption and emission to better visualize the respective trends. The ligand concentration was 2.3×10^{-6} M, the solvent was ACN, and excitation was at 310 nm (isosbestic point). Inset: Absorbance (left) and fluorescence intensity (right) at selected wavelengths, i.e., the maximum of the acceptor chelate absorption band (438 nm) and the ligand's emission band (510 nm) as a function of Cu(II) concentration.

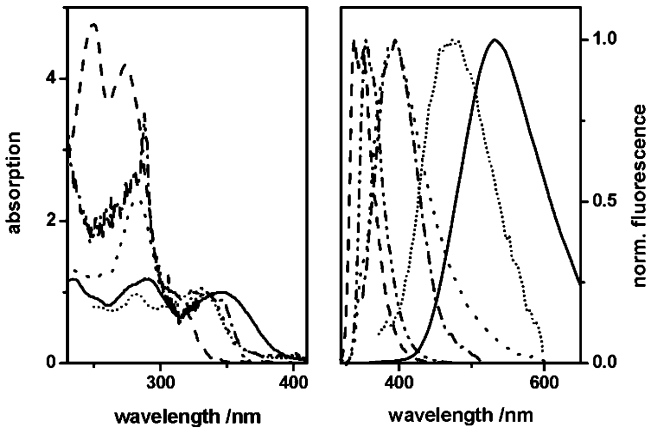

Figure 6. Comparison of normalized absorption (left) and normalized emission (right) spectra of selected cation complexes and protonated species of bpb-R: bpb-R with R = DMA (**4**) (solid line); $Cu^{2+}\supset\mathbf{4}\subset Cu^{2+}$ (short dotted line, 5:1 Cu^{2+}); **4** with protons and Cu(II) (dash−dotted line, 1:100 H^+ followed by addition of 10:1 Cu^{2+}; $H^+\supset\mathbf{4}\subset Cu^{2+}$); completely protonated **4** (dash−dot−dotted line, 100:1 H^+; $H^+\supset\mathbf{4}\subset x H^+$); bpb-R with R = H (**2**) (dashed line); and monoprotonated **2** (dotted line, 8:1 H^+). The probe concentration was 2.3×10^{-6} M, the solvent was acetonitrile, and excitation was at 310 nm. The metal ion and/or proton to ligand concentration ratios used are given in the parentheses. The absorption spectrum of $H^+\supset\mathbf{4}\subset x H^+$ that resembles that of monoprotonated **2** was omitted for reasons of clarity.

other. For the spectroscopic features discussed in the following sections, we always assume complete donor coordination. Concerning the spectroscopic properties of A- and D-bound bpb-DMA and bpb-A15C5, of special interest here is the degree of resemblance between the emission properties of D- and A-coordinated **4** and **5** and monoprotonated **2** which provides a measure for the size of the interaction between the donor receptor and the metal ion in the excited state. Close resemblance points to complete engagement of the nitrogen lone pair of the donor receptor in the D- and A-bound species, whereas an emission spectrum that is barely blue shifted compared to that of the A-coordinated probe indicates a disruption of the cation−nitrogen bond following excitation of the complex.

Bifunctionality Studies with bpb-DMA. To evaluate the potential of **4** for signaling of a single guest over an extended dynamic range, we investigated its consecutive A- and D-coordination to Cu(II). The corresponding Cu(II)-dependent absorption and emission spectra are depicted in Figure 5. At low Cu(II) concentrations of ca. M:L ≤ 1, exclusive formation of the acceptor chelate occurs as follows from the appearance of a broad and red shifted absorption band of CT nature centered at 437 nm and the disappearance of the probe's emission at 515 nm. A further increase in Cu(II) concentration leads to a decrease of the newly formed A-chelate absorption band. Furthermore, at higher Cu(II) to ligand concentration ratios, a very weak, blue shifted emission at ca. 474 nm appears. Most likely, this fluorescence originates from D- and A-coordinated **4**, i.e., $Cu^{2+}\supset\mathbf{4}\subset Cu^{2+}$, as derived, e.g., by a comparison of the emission spectra of $\mathbf{1}\subset H^+$, **4**, and this species depicted in Figure 6. Due to the very weak emission of the Cu(II)-bound species, no attempts were made to determine its fluorescence quantum yield and fluorescence lifetime. The dependence of the A-chelate's absorption and the probe's emission band on Cu(II) concentration follows from the insets in Figure 5. The former illustrates the extended dynamic range of **4** provided by its bifunctionality. The complexation constant for D-coordination of $\mathbf{4}\subset Cu^{2+}$ is determined to 4.8 (log K_s) from absorption measurements assuming a 1:1 stoichiometry for D-coordination.

Bimodal Cu(II) sensing by **4** encouraged us to investigate the ability of this fluorescent reporter to simultaneously recognize two analytes. Here, we chose Cu(II) and protons. As displayed in Figure 6, addition of protons to the Cu(II) acceptor chelate of **4** leads to a blue shift in absorption and emission. The hypsochromically shifted emission band located at ca. 395 nm strongly resembles the fluorescence of monoprotonated **2**. This species is tentatively assigned to $H^+\supset\mathbf{4}\subset Cu^{2+}$ as the much weaker coordination of Cu(II) to the dimethylamino group compared to the terpyridine moiety renders substitution of DMA-coordinated Cu(II) for protons more plausible than substitution of terpyridine-bound Cu(II) for protons. Since the emission of Cu(II)- and proton-coordinated **4** is only very weak, we did not attempt to determine its fluorescence quantum yield and fluorescence lifetime or to perform further experiments to clarify its exact chemical nature and the formation of mixed complexes. However, we investigated the reversibility of proton and Cu(II) coordination of **4**. The spectroscopic effects observed upon addition of protons to the Cu(II) acceptor chelate of **4** are comparable to those accompanying the addition of Cu(II) to donor- and acceptor-protonated bpb-DMA. Obviously, protons can substitute DMA-coordinated Cu(II) and Cu(II) can replace terpyridine-bound protons.

Bifunctionality Studies with bpb-A15C5. Based on the results of acceptor coordination of **5** and the complexation studies performed with **4**, D- and A-coordination of **5** is studied with the representative metal ion Ca(II) and the cation pair Zn(II) and Na(I). Consecutive binding of the A-receptor and the D-receptor of **5** to Ca(II) is depicted in Figure 7. For low Ca(II) concentrations, i.e., for M:L ratios ≤ 10:1, Ca(II) binding involves exclusively the terpyridine acceptor moiety as follows from the Ca(II)-induced red shifts in absorption (lowest energy band; left upper panel) and emission (middle and right upper panels); see Figure 7 and Table 1. The lowest energy CT-type absorption band of the calcium acceptor chelate is centered at 394 nm and its emission band is at 592 nm, respectively, with

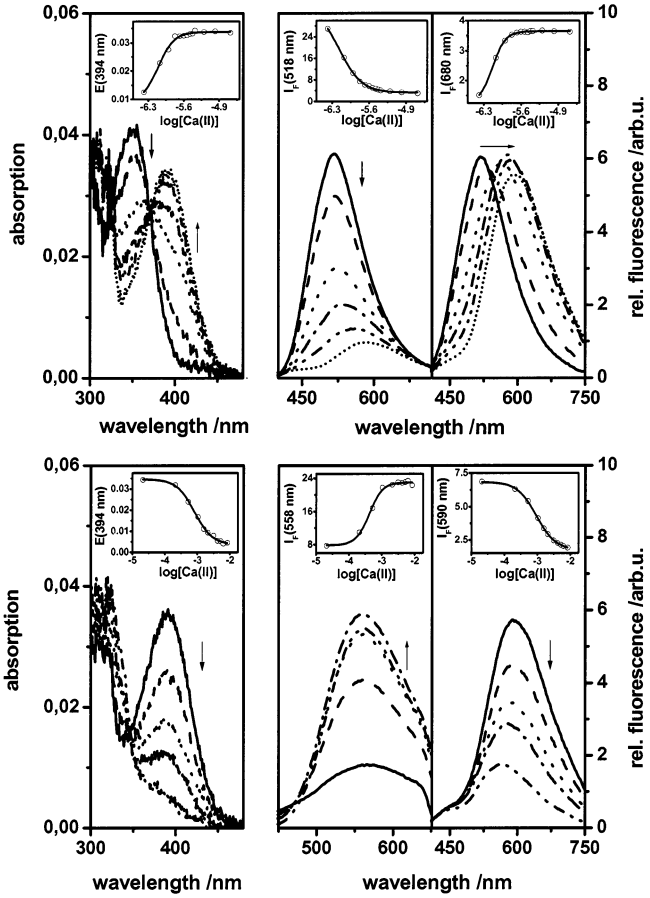

Figure 7. Bifunctionality studies with bpb-A15C5 (**5**) and Ca(II). Upper part: Absorption (left) and emission (middle, right) spectra measured at low metal ion to ligand concentration ratios, i.e., Ca(II):**5** = 0:1 (solid line), 0.2:1 (dashed line), 0.4:1 (dotted line), 0.6:1 (dash−dotted line), 1:1 (dash−dot−dotted line), and 10:1 (short dotted line). Lower part: High metal ion to ligand concentration ratios, Ca(II):**5** = 10:1 (solid line), 250:1 (dashed line), 500:1 (dotted line), 750:1 (dash−dotted line), and 4000:1 (dash−dot−dotted line). The ligand concentration was 2×10^{-6} M, the solvent was ACN, and excitation was at 372 nm (isosbestic point; middle panel) and 394 nm (acceptor chelate band; right panel). Insets: Absorbance at 394 nm (top and bottom, left) and fluorescence intensity at different characteristic emission wavelengths (λ_{em}) (top, middle: λ_{em} = 518 nm, λ_{exc} = 372 nm; top, right: λ_{em} = 680 nm, λ_{exc} = 394 nm; bottom, middle: λ_{em} = 558 nm, λ_{exc} = 372 nm; top, right: λ_{em} = 590 nm, λ_{exc} = 394 nm) as a function of Ca(II) concentration (log [Ca(II)]).

the size of the chelation-induced spectral shifts reflecting the strongly electron withdrawing character of the Ca(II)-bound terpyridine acceptor. The clear course of Ca(II) ligation is revealed by an isosbestic point at 372 nm for M:L ratios ≤ 10:1. Coordination of the A-receptor of bpb-A15C5 to Ca(II) results in a considerable diminution in fluorescence quantum yield as follows from the middle panel in the upper part of Figure 7 and Table 1, which displays the terpyridine ligation-induced changes in the fluorescence of **5** for excitation at the isosbestic point. Moreover, the fluorescence lifetime is strongly reduced from 5.7 to 0.7 ns (see Table 2) and k_{nr} is enhanced by a factor of ca. 10. k_f is more or less unaffected. A further increase in Ca(II) concentration results in the consecutive complexation of the azacrown donor receptor yielding $Ca^{2+}\supset\mathbf{5}\subset Ca^{2+}$ as indicated by the disappearance of the absorption band of the Ca(II) acceptor chelate (right lower panel) and a blue shift of its emission band from 592 to 565 nm (middle and right lower panels); see Figure 7. Furthermore, as summarized in Table 2, the fluorescence quantum yield and the fluorescence lifetime of $Ca^{2+}\supset\mathbf{5}\subset Ca^{2+}$ are both enhanced by a factor of ca. 3 with respect to $\mathbf{5}\subset Ca^{2+}$, k_f increases slightly, and k_{nr} is reduced by a factor of ca. 3. The complexation constant of donor coordination is determined to 3.0 (log K_s) assuming formation of a 1:1 complex and independent donor chelation of A-bound **5**. The insets in the upper and lower panels of Figure 7 highlight the concentration dependence of intensity changes in absorption and in emission at selected wavelengths, thereby underlining the analytical potential of such a bifunctional CT-operated probe, i.e., the extended concentration range for monitoring of the analyte.

bpb-A15C5 is also suited for the simultaneous recognition of two different chemical inputs as, for example, revealed for Zn(II) and Na(I). Addition of Zn(II) to $Na^{+}\supset\mathbf{5}$ yields a species with an absorption band located at ca. 320 nm and a very weak fluorescence centered at ca. 585 nm. The absorption and emission bands of the zinc A-chelate of **5**, however, are centered at 427 and 617 nm (see Table 1). This newly formed species is tentatively assigned to $Na^{+}\supset\mathbf{5}\subset Zn^{2+}$. Due to its very weak emission, no attempts were made to determine its fluorescence quantum yield and fluorescence lifetime.

3.4. Spectroscopic Properties of the Cation Complexes of bpb-R: Comparison and Discussion within the Framework of Neutral and Ionic D−A Biphenyls. As has been illustrated in sections 3.1, 3.2, and 3.3 on acceptor, donor, and A- and D-coordination of bpb-R, this family of fluorescent reporters reveals strong and coordination-site-specific chelation-induced shifts in energy and intensity of the absorption and emission bands with protons, alkaline earth metal ions such as Ca(II), and quenching and nonquenching transition metal ions such as Zn(II), Hg(II), and Cu(II). These fluoroionophores not only are rare examples for true ratiometric emission sensing with CT-operated sensor molecules,[12,67] but also display even analytically favorable red shifts in the terpyridine-coordinated state due to the chelation-induced increase in acceptor strength. In the case of alkali metal ions such as Na(I) that exclusively bind to the monoazacrown D-receptor of **5**, strong changes in absorption, yet only slight changes in emission, occur as is typical for D-binding of this type of fluorescent probe. This behavior points to a disruption of the nitrogen−cation bond in the excited state followed by either fast cation release after formation of the CT species as observed for DCM crown or formation of a solvent separated cation−probe pair similarly to DCS crown.[12,68] When equipped with two binding sites, the bifunctional bpb-R molecules **4** and **5** are capable of signaling two different inputs, X_1 and X_2. These inputs can be either two different analytes or different concentration regimes of a single analyte, thereby yielding an extended dynamic range of probe operation.

Spectroscopic Properties of the Acceptor Chelates of bpb-R: Influence of the CT Character of the Probe and the Electronic Nature of the Cation. To derive structure−property relationships for biphenyl-type sensor molecules capable of ratiometric emission sensing, the spectroscopic features of the acceptor chelates of bpb-R are compared with respect to (i) the CT character of the complexes that reveals both the donor strength of R and the strength of the analyte−terpyridine interactions and (ii) the influence of the cation's electronic nature, i.e., its potential to act as fluorescence quencher via the heavy atom effect, paramagnetism, energy, or electron transfer.[39] For the interpretation of the underlying photophysical processes, we focus on the acceptor chelates of nonquenching Ca(II) and Zn(II) (see sections 3.1. and 3.3) to exclude contributions from metal ion related fluorescence-quenching effects and consider the spectroscopic properties of neutral and ionic D−A biphenyls

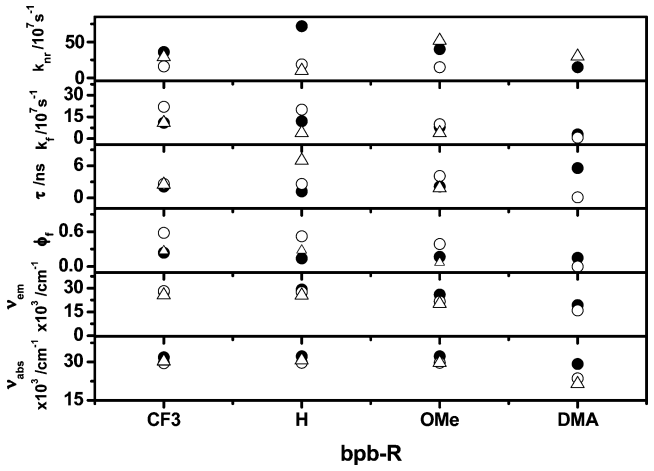

Figure 8. Spectroscopic properties of bpb-R and its zinc complexes as a function of the donor strength of R (R = CF_3, **1**; H, **2**; OMe, **3**; DMA, **4**): bpb-R (filled circles), zinc complex (open circles). The solvent was ACN. For comparison, the monoprotonated bpb-R species (open triangles) are also included. For acceptor-protonated bpb-DMA, no emission could be detected.

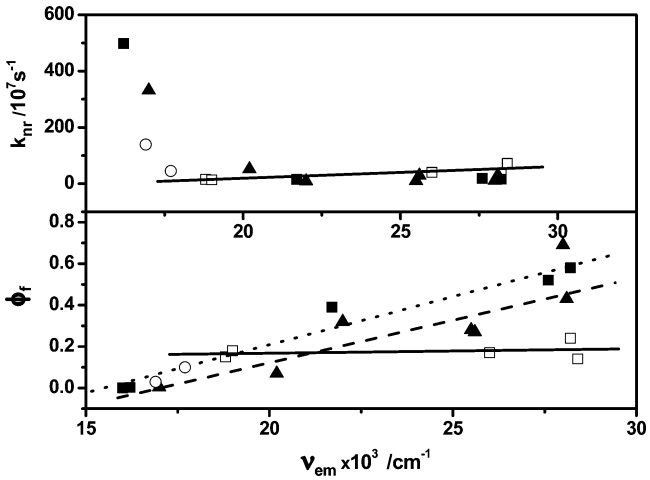

Figure 9. Fluorescence quantum yield ϕ_f and nonradiative rate constant k_{nr} of neutral, protonated, and Zn(II)-coordinated bpb-R as function of the spectral position of the respective emission maximum: neutral bpb-R (**1**−**5**, see Scheme 1) (open squares); protonated bpb-R, i.e., monoprotonated and doubly protonated bpb-R as well as A- and D-protonated $H^+\supset$**4**$\subset x H^+$ (filled triangles); and A-chelates with Zn(II) (filled squares). For comparison, **5**$\subset Ca^{2+}$ and $Ca^{2+}\supset$**5**$\subset Ca^{2+}$ (open circles) are also included. The lines are only guides for the eye.

derived from the literature,[45,50,52,69,70] some of which are shown in Scheme 2, as well as the spectroscopic features of monoprotonated and monocoordinated D−D biphenyl-type sensor molecule **9**[19] and protonated bpb-R.[38]

For each cation studied, the size of the coordination-induced spectral shifts in bpb-R depend on R in the following order: CF_3 < H < OMe ≪ DMA ≈ A15C5 in absorption and CF_3 < H ≪ DMA ≈ A15C5 ≪ OMe in emission (see section 3.1 and Figure 3, Figure 4, and Table 1). The coordination-induced spectral shifts of the lowest energy absorption band and the emission band of each fluoroionophore typically increase in the order Ca(II) < Zn(II) ≤ Hg(II) ≤ Cu(II). The size of the spectral changes in absorption and emission accompanying acceptor coordination are indicative of the strength of the coordination of the respective analyte to the terpyridine moiety for a given substituent R. The observation that the magnitude of the monoprotonation-induced spectral changes in absorption are smaller than the corresponding chelation-induced effects whereas in emission this trend is reversed (see Table 1 and Figure 4) is ascribed to the underlying design concept of this family of fluorescent reporters and the type of interaction between the terpyridine acceptor and the analyte. Binding of metal ions to terpyridine typically occurs via coordinative bonds, whereas in the case of acceptor protonation a covalent bond is formed between the proton and a terpyridine nitrogen atom, leading to a stronger decrease in electron density of the acceptor and thus enhancement in CT character of the sensor molecule. An alternative explanation may be a change in the location and number of cation interactions from the ground state to the excited state. In any case, this underlines the influence of the size of the coordination-induced increase in acceptor strength on the spectroscopic properties of the resulting species for such A-coordinating intrinsic probes. The spectroscopic properties of the zinc complex of **1** are astonishing, displaying a chelation-induced red shift in absorption and a blue shift in emission similar to doubly protonated **1**.[38] The exact nature of this species is currently being investigated by us.

Comparison of Zinc and Calcium Complexes to Neutral and Protonated bpb-R. The size of the fluorescence quantum yields of the acceptor chelates is controlled by both the CT character of the complexed sensor molecule and the potential of the bound cation to act as fluorescence quencher as follows from Tables 1 and 2 as well as from Figures 8 and 9. From the bottom to the top layer, Figure 8 compares the (low energy) absorption and emission maxima as well as the fluorescence quantum yields, fluorescence lifetimes, and the radiative and nonradiative rate constants of the zinc complexes of bpb-R, monoprotonated bpb-R, and the parent sensor molecules. The most striking features of this figure are (i) the high fluorescence quantum yields and k_f values of the zinc complexes of **1** and **2** and—less pronounced—also of **3**, which considerably exceed those of the corresponding neutral ligands and monoprotonated species, (ii) the considerable decrease in fluorescence quantum yield occurring for Zn(II)-bound **4**, and (iii) the strong chelation- and protonation-induced alterations in k_{nr}; see also Figure 9. Figure 9 displays the fluorescence quantum yields and nonradiative rate constants of bpb-R, its zinc acceptor chelates, and its protonated analogues as a function of the spectral position of the respective emission maxima that provides a measure for the species' CT character. For comparison purposes, **5**$\subset Ca^{2+}$ and $Ca^{2+}\supset$**5**$\subset Ca^{2+}$ are included in this figure. As follows from Figure 9 and Table 2, in all cases, the size of the fluorescence quantum yields and the size of the radiative rate constants decrease with a reduction in energy of the emission maximum within each series of chemically related species, for example, zinc complexes or monoprotonated bpb-R. Zinc coordination as well as monoprotonation and double protonation of the terpyridine acceptor leads to a sizable decrease in k_{nr} for **1** and **2**, whereas in the case of **3** zinc coordination reduces k_{nr} by a factor of ca. 3 while monoprotonated **3** with its red shifted fluorescence already displays a slight increase of k_{nr}. For **4** as well as for **5**, k_{nr} is strongly enhanced upon zinc binding; see Table 2 and Figure 9. Acceptor-protonated **4** is more or less nonemissive. The nonradiative rate constants of both D- and A-protonated **4** and D- and A-coordinated **5**, i.e., $Ca^{2+}\supset$**5**$\subset Ca^{2+}$, that display either strongly or slightly blue shifted emission spectra are medium-sized.

Spectroscopic Features of the Acceptor Chelates of bpb-R within the Framework of Neutral and Ionic D−A Biphenyls. The spectroscopic features of the cation complexes of bpb-R can be understood within the framework of neutral and ionic biphenyls such as **6**, **6a**, **7**, and **8** depicted in Scheme 2.[45,52,70]

For these D−A biphenyls substituted with sufficiently strong D−A substituents, a red shift in the spectral position of the absorption and emission bands—resulting as a function of increasing solvent polarity—correlates with a diminution of both the radiative rate constants and the fluorescence quantum yields due to the enhanced formation of a forbidden CT state of twisted conformation. This opens up a strong nonradiative fluorescence deactivation pathway which is typically indicated by small radiative and large nonradiative rate constants.[52] For a given donor substituent R, the CT character of ionic D−A biphenyls, which present model systems for A-ccordination, is already more pronounced compared to their neutral counterparts,[70] and the tendency toward TICT formation[70] is enhanced. Accordingly, similar effects are expected to occur for A-coordinated biphenyl-type fluorescent reporters. The high values of k_f of the zinc complexes of **1** and **2** and the intermediate size of k_f of $\mathbf{3}\subset Zn^{2+}$ suggest that for these acceptor chelates, however, the main conformation of the complexed bpb-R sensor molecule is planar. The chelation-induced reduction in k_{nr} for **1**−**3** that contradicts the energy gap rule, which predicts an increase of k_{nr} with a narrowing of the S_1-S_0 energy gap,[71,72] is remarkable. The corresponding Ca(II) complexes are expected to display similar effects in k_f and k_{nr}, though not presented here. This discussion of an anti-energy gap rule behavior, though plausible and tempting, is, however, subject to certain simple photophysical assumptions[73] that have been detailed in part 1 of this series.[38]

Such a comparatively rare anti-energy gap law dependence is revealed qualitatively for instance by sterically hindered **6a**[45] as well as by **4** and **5** and, very pronounced, by protonated **2**.[38] In the case of protonated **2**, we attribute the sizable reduction in k_{nr} to contributions from protonation-induced planarization and rigidization of the terpyridine fragment.[38,74] As cation coordination of the terpyridine acceptor—dependent on the strength of the cation−receptor interactions and type of cation−nitrogen bonds—introduces a smaller charge into the terpyridine moiety but simultaneously enhances its rigidity compared to protonation, this provides the basis for even more favorable fluorescence effects for nonquenching metal ions such as Zn(II) and Ca(II) and the bpb-R family. This counterbalancing effect most likely accounts for the strong emission of the zinc and calcium complexes of **1**−**3** in addition to the chelation-enhanced k_f values. Forbidden emission from a CT state of twisted conformation results only for all the A-coordinated species derived from **4** and **5** equipped with strong donors as indicated by their small radiative rate constants; see Table 2 and Figure 9. The weak emission of the acceptor chelates of **4** and **5** corresponds with their strongly red shifted emission bands and increased nonradiative rate constants in accordance with the energy gap rule.

Acceptor coordination of bpb-R to potentially quenching metal ions[39] is always accompanied by a strong diminution of the probe's fluorescence and by very small radiative rate constants, as follows from Tables 1 and 2 representatively for Hg(II) and Cu(II) (see section 3.1). For these quenching metal ions, realization of a sizable emission of the complexes with intrinsic A-coordinating probes is more straightforwardly conceivable for D−A systems where the D−A charge transfer reaction results in a strongly emissive CT state of predominantly planar conformation.[21] This is suggested also by the spectroscopic features of the D−D biphenyl type sensor molecule **9** that undergoes a chelation-enhanced fluorescence with the classical fluorescence quencher Hg(II).[19] For the bpb-R family, a suitable design strategy that is currently being tested by us seems to be the reduction of the strength of the A-receptor, for instance by exchanging the electron-withdrawing 2- and 6-pyridyl substituents within the terpyridine moiety for electron-donating 2- and 6-substituents such as thienyl groups, thereby preserving the otherwise advantageous properties connected with acceptor complexation of these fluorescent reporters.

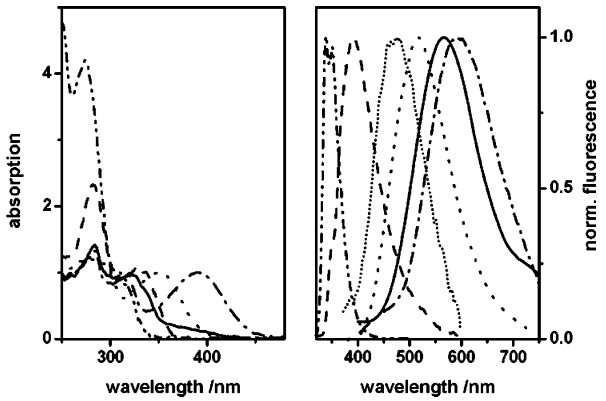

Figure 10. Comparison of the spectroscopic properties of A- and D-coordinated bpb-DMA (**4**) and bpb-A15C5 (**5**) for representative analytes: normalized absorption (left) and emission (right) spectra of **5** (dotted line), $\mathbf{5}\subset Ca^{2+}$ (dash−dotted line, 10:1 Ca^2), $Ca^{2+}\supset\mathbf{5}\subset Ca^{2+}$ (solid line, 4000:1 Ca^{2+}), and $Cu^{2+}\supset\mathbf{4}\subset Cu^{2+}$ (short dotted line, 5:1 Cu^{2+}). The ligand concentration was 2×10^{-6} M, the solvent was ACN, and excitation was at the longest wavelength absorption band. For comparison, the corresponding spectra of bpb-R with R = H (**2**) (dash−dot−dotted line) and $\mathbf{2}\subset H^+$ (dashed line, 8:1 H^+) are included. Only selected absorption spectra are shown for reasons of clarity. The emission spectrum of $H^+\supset\mathbf{4}\subset Cu^{2+}$ (not shown) resembles that of $\mathbf{2}\subset H^+$.

Spectroscopic Properties of A- and D-coordinated bpb-R. As illustrated in section 3.3, the spectral position of the absorption and emission maxima of A- and D-coordinated **4** and **5** is controlled by the coordination-induced changes in CT character and thus the size of the analyte−receptor interactions in the ground state and excited state. This is highlighted in Figure 10, which compares the absorption and fluorescence spectra of **5**, $\mathbf{5}\subset Ca^{2+}$, $Ca^{2+}\supset\mathbf{5}\subset Ca^{2+}$, $Cu^{2+}\supset\mathbf{4}\subset Cu^{2+}$, and $H^+\supset\mathbf{4}\subset Cu^{2+}$ to the corresponding spectra of **2** and $\mathbf{2}\subset H^+$. The latter two molecules act as model systems for complete abstraction of the electron lone pair of the nitrogen atom of the D-receptor in noncoordinated and A-bound bpb-DMA and bpb-A15C5. As follows from Figure 10 and Table 1, the absorption spectra of A- and D-coordinated **4** and **5** in all cases resemble the absorption spectrum of monoprotonated **2**, peaking at 327 nm. In contrast, the spectral position of the emission bands of A- and D-coordinated **4** and **5** strongly depend on the chemical nature of the analyte(s) bound with maxima at 395, 474, 565, and 585 nm resulting for $H^+\supset\mathbf{4}\subset Cu^{2+}$, $Cu^{2+}\supset\mathbf{4}\subset Cu^{2+}$, $Ca^{2+}\supset\mathbf{5}\subset Ca^{2+}$, and $Na^+\supset\mathbf{5}\subset Zn^{2+}$, respectively. The emission bands of strongly emissive D- and A-protonated **4** (not shown in Figure 10) and $\mathbf{2}\subset H^+$ reveal maxima at 356 and 392 nm. The analyte-specific emission of A- and D-coordinated bpb-R, which is intriguing for such a CT-operated sensor molecule, is encouraging for the spectral discrimination between different analytes or species. Most likely, photorelease or excited-state decoordination[12,68] of the donor-bound metal ions Cu(II), Ca(II), and Na(I) in A-coordinated bpb-R accounts for these analytically favorable effects, with the size of the D-coordination-induced blue shift in emission revealing the strength of the cation−nitrogen bond in the excited state of the doubly coordinated fluoroionophore. Obviously, aminophilic Cu(II) is more strongly bound than Ca(II) and Na(I). A direct comparison of these fluorescence effects is, however, partly hampered by

the fact that, within the underlying probe design concept, the CT character—and thus the spectroscopic properties of the resulting species—are controlled by both the A- and the D-coordination-induced changes in acceptor and donor strength. As follows, e.g., from the spectroscopic data summarized in Table 1, for acceptor chelation of **4** and **5** to Cu(II), Ca(II), and Zn(II), the size of the terpyridine−analyte interactions and thus the strength of the acceptor moiety differ slightly, which accordingly affects donor coordination.[75] As indicated by the close resemblance between the emission spectra of $\mathbf{2}\subset H^+$ and $H^+\supset\mathbf{4}\subset Cu^{2+}$, donor protonation induces a more or less complete withdrawal of the nitrogen lone pair of the donor receptor from the probe's π-electron system. As a very favorable fact, in addition to the comparatively strong spectral changes in emission, the bpb-R sensor molecules yield considerable changes in fluorescence lifetime contrary to the majority of simple fluorescent reporters with integrated donor receptors.[8,12] For instance, **5**, $\mathbf{5}\subset Ca^{2+}$, and $Ca^{2+}\supset\mathbf{5}\subset Ca^{2+}$ display fluorescence lifetimes of 5.7, 0.7, and 2.0 ns (see Table 2) that, together with the spectral information from absorption and emission measurements, provide an extra parameter for the discrimination among these three species.

The spectroscopic properties of $Ca^{2+}\supset\mathbf{5}\subset Ca^{2+}$, i.e., its red emission in combination with its comparatively high fluorescence quantum yield of 0.10 exceeding that of $\mathbf{5}\subset Ca^{2+}$ by a factor of ca. 3, are intriguing; see Tables 1 and 2 and Figures 9 and 10. A comparison of the spectroscopic properties of $Ca^{2+}\supset\mathbf{5}\subset Ca^{2+}$, $H^+\supset\mathbf{4}\subset xH^+$, **5**, and $\mathbf{5}\subset Ca^{2+}$ reveals strong differences in the size of the fluorescence quantum yields as well as radiative and nonradiative rate constants aside from the spectral differences in absorption and emission already discussed. The strongly blue shifted emission of $H^+\supset\mathbf{4}\subset xH^+$ that resembles that of unbound bpb-H[38] occurs from an allowed planar CT state as indicated by the high k_f value, whereas in the case of $Ca^{2+}\supset\mathbf{5}\subset Ca^{2+}$ both the spectral position of the emission band and the size of k_f point to emission from a forbidden CT state of twisted conformation. Its comparatively high fluorescence quantum yield resulting in a fluorescence enhancement is obviously connected with a decrease of the nonradiative rate constant by a factor of ca. 3 initiated by D-coordination of $\mathbf{5}\subset Ca^{2+}$. This is astonishing with respect to the blue shift in emission for $Ca^{2+}\supset\mathbf{5}\subset Ca^{2+}$ of only 800 cm^{-1} as compared to $\mathbf{5}\subset Ca^{2+}$. See Tables 1 and 2 and Figures 7 and 10, which may, however, point to (partial) donor decoordination in $Ca^{2+}\supset\mathbf{5}\subset Ca^{2+}$.[12] Similar to **6a**[45] as well as to **4** and **5** and protonated **2** discussed in part 1 of this series,[38] $Ca^{2+}\supset\mathbf{5}\subset Ca^{2+}$ seems to be an exception from the energy gap rule.[71,72,73] In any case, this underlines the analytical potential of coordination-induced switching between energy gap and anti-energy gap law type behavior for the realization of a chelation-induced fluorescence enhancement with CT-operated sensor molecules.

3.5. Bifunctionality of and Bimodal Sensing with bpb-R and Potential as Molecular Switches. *Bifunctionality.* bpb-DMA and bpb-A15C5 are suited for multimodal analyte recognition via coordination-site-specific, spectroscopically different outputs as follows from Figures 5−7, Figure 10, Table 1, and Table 2. Both sensor molecules can principally form four spectroscopically distinguishable states: the *unbound state*, the *A-coordinated state* with red shifted absorption and emission spectra compared to the unbound state, the *D-coordinated state* with blue shifted absorption spectra compared to uncomplexed bpb-R and barely affected emission spectra, and the *D- and A-coordinated state*. As representatively derived for selected analytes and bpb-DMA and bpb-A15C5, the four- or three-state sensing schemes *none*, *analyte X_1*, *analyte X_2*, and *analytes X_1 and X_2* or *none*, *little*, and *many* can be exploited for the optical transduction of two chemical inputs or two concentration regimes of a single analyte. The fluorescence quantum yield controlled output of the different states of bound bpb-R are determined by the CT character of the complex, the electronic nature of the coordinated analyte, and the chelation-induced changes in k_f and k_{nr}. A sizable emission results only for the parent ligands and the A- and D-coordinated species with nonquenching metal ions and protons.

This type of bifunctional sensing relies not only on clearly distinguishable spectroscopic features of the differently coordinated species, but similarly on complexation constants of the two binding sites that differ considerably. Both criteria are obviously fulfilled for bpb-DMA and bpb-A15C5 and the selected analytes. Here, it must be kept on mind, however, that the size of the complexation constant of donor coordination is affected upon acceptor coordination, i.e., weakened compared to that of neutral bpb-R due to the A-chelation-induced reduction in electron density at the donor's nitrogen atom. This complicates the design of such bifunctional CT-operated sensor molecules in comparison to ET-operated electronically decoupled devices.[29]

Exploitation of the Parameter Fluorescence Lifetime. The selectivity of fluorescent reporters such as the bpb-R family can be increased by exploitation of the analyte-specific parameter fluorescence lifetime in addition to the hitherto discussed coordination-induced spectral effects. The impact of this parameter, though not optimized yet for these sensor molecules, follows, e.g., for sensor molecule **5** principally from a comparison of the photophysical properties of its complexes with calcium, zinc, and sodium summarized in Tables 1 and 2. Although the spectral properties of the Ca(II) and the Zn(II) acceptor chelates are very similar, these species can be discriminated by their lifetimes and distinguished from longer lived $Ca^{2+}\supset\mathbf{5}\subset Ca^{2+}$. The Na(I) complex of **5** is easily distinguished from the Ca(II) and Zn(II) acceptor chelates and from $Ca^{2+}\supset\mathbf{5}\subset Ca^{2+}$ by its blue shifted fluorescence and its increased fluorescence lifetime. The fluorescence lifetime can also be used to discriminate the Na(I) complex of **5** from its parent ligand. Finally, $Na^+\supset\mathbf{5}\subset Zn^{2+}$ can be identified and distinguished from the other species by its specific combination of emission and absorption maxima.

*Potential of **4** and **5** as Molecular Switches and Logic Gates Operated with Metal Ions and Protons.* The design of molecular switches and molecular equivalents of logic gates that both convert input stimulations into output signals with intrinsic protocols following the principles of binary logic is a straightforward extension of studies on fluorescent sensor molecules.[5,6,28,76,77] The analysis of the logic behavior of such devices, however, requires proper assignment of threshold values and logic conventions to their input and output signals. Different types of systems that perform logical operations with chemical inputs and provide optical outputs have been reported up to now including, e.g., AND,[78] OR,[79] NOR,[80] INHIBIT,[81] YES,[82] and NOT[83] logic gates. These devices are typically ET-operated and respond to combinations of protons and alkali or alkaline earth metal ions.[29,84] In contrast to the general interest in systems that undergo clearly distinguishable changes of different measurable fluorescence parameters specific for a certain chemical input, examples for CT-operated logic gates are comparatively rare.[21,35] As has been suggested by the protonation studies detailed in part 1 of this series[38] and the previously discussed spectroscopic properties of A-coordinated, D-coordinated, and A- and D-

coordinated bpb-DMA and bpb-A15C5, principally, CT-operated biphenyl-type molecules with integrated A- and D-receptors seem to be suited for logic operation with the proper choice of the absorption, excitation, and emission wavelengths due to their strong input-controlled changes in intensity, energy, and fluorescence lifetime.[28,30] For this type of application, however, future developments of the bpb-R series need to be directed toward more selective receptors. One ongoing approach is the substitution of the terpyridine acceptor receptor for a more selective one, e.g., a 2,6-bis(2-thienyl)pyridine binding site.[14,85] In any case, like many other fluorescent reporters and molecular switches undergoing chelation-induced fluorescence quenching, bpb-R can, for instance, transduce the chemical input Cu(II) or Hg(II) into the disappearance of its emission, thereby switching the fluorescence measured at the ligand's emission maximum from a high to a low output.[39] For bpb-A15C5 and bpb-DMA, the formation of a red shifted absorption band upon acceptor chelation can be exploited for a NOT gate.[76]

4. Summary and Conclusion

The bpb-R family presents an elegant, yet simple approach to CT-operated cation- and pH-responsive fluorescent reporters that reveal analytically favorable complexation-induced modulations in energy, in absorption, and in emission as a prerequisite for true ratiometric emission signaling as well as changes in fluorescence quantum yield and fluorescence lifetime. This underlines the advantage of acceptor vs donor coordination for such intrinsic fluoroionophores that otherwise display strong analyte-mediated effects only in absorption. Biphenyl molecules substituted with integrated D- and A-receptors, such as bpb-DMA and bpb-A15C5, belong to the few examples of CT-operated bifunctional fluorescent probes capable of bi- and multimodal spectroscopic analyte recognition. This principally provides the basis for three- or four-state sensing schemes of two different inputs, i.e., either a single analyte at different concentration regimes or two chemically different species. The photophysics of neutral bpb-R, their acceptor chelates, and acceptor- and donor-coordinated bpb-DMA and bpb-A15C5 are governed by CT control of an excited-state barrier toward formation of a CT state with forbidden emission, switching between anti-energy and energy gap law type behavior, and the electronic nature of the ligated metal ion. This accounts for the astonishingly high fluorescence quantum yields of both the acceptor chelates of bpb-R equipped with weak or medium-sized donors and the red emission of D- and A-coordinated bpb-R for nonquenching metal ions. Partial photorelease or excited-state decoordination occurring for D- and A-bound bpb-DMA and bpb-A15C5 provides the basis for the communication of the D-coordinated species by analyte-specific emission maxima of doubly coordinated bpb-DMA and bpb-A15C5.

Acknowledgment. Financial support from the Deutsche Forschungsgemeinschaft (DFG; Grants RE387/8-3 and 436-UKR113/24-3) is gratefully acknowledged. We are indebted to Dr. D. Pfeifer for provision of the spectral correction curves, Dr. K. Rurack for help with the spectroscopic studies, Dr. W. Weigel for help with the time-resolved-fluorescence measurements, Mrs. A. Rothe for assistance with the figures, and BESSY II for beam time.

References and Notes

(1) Rurack, K. *Spectrochim. Acta, Part A* **2001**, *57A*, 2161 and references therein.

(2) For example, see: *Chemosensors of Ion and Molecule Recognition*; Desvergne, J. P., Czarnik, A. W., Eds.; Kluwer Academic Publishers: Dordrecht, Netherlands, 1997, and specific reviews referenced in the various chapters.

(3) Wiegmann, T. B.; Welling, L. W.; Beatty, D. M.; Howard, D. E.; Vamos, S.; Morris, J. A. *J. Physiol.* **1993**, *265*, C1184. Salvador, J. M.; Inesi, G.; Rigaud, J. L.; Mata, A. M. *Biol. Chem.* **1998**, *273*, 18230. Vo-Dinh, T.; Viallet, P.; Ramirez, L.; Pal, A.; Vigo, J. *Anal. Chim. Acta* **1994**, *295*, 67. Hirshfeld, K. M.; Toptygin, D.; Grandhige, G.; Packard, B. Z.; Brand, L. *Biophys. Chem.* **1998**, *71*, 63.

(4) *New Trends in Fluorescence Spectroscopy: Applications to Chemical and Life Sciences*; Valeur, B., Brochon, J.-C., Eds.; Springer: Berlin, 2001. More specific reviews are referenced in the various chapters.

(5) *Molecular Switches*; Feringa, B. L., Ed.; Wiley-VCH GmbH: Weinheim, 2001.

(6) de Silva, A. P.; Fox, D. B.; Moody, T. S.; Weir, S. M. *Trends Biotechnol.* **2001**, *19*, 29.

(7) Rurack, K.; Resch-Genger, U. *Chem. Soc. Rev.* **2002**, *31*, 116.

(8) For example, see special issue on Luminescent Sensors. *Coord. Chem. Rev.* **2000**, *205*.

(9) de Silva, A. P.; Gunaratne, H. Q. N.; Gunnlaugson, T.; Huxley, A. J. M.; McCoy, C. P.; Rademacher, J. T.; Rice, T. E. *Chem. Rev.* **1997**, *97*, 1515 and references therein.

(10) For example, see: Jonker, S. A.; van Dijk, S. I.; Goubitz, K.; Reiss, C. A. *Mol. Cryst. Liq. Cryst.* **1990**, *183*, 273. Kollmannsberger, M.; Rurack, K.; Resch-Genger, U.; Daub, J. *J. Phys. Chem. A* **1998**, *102*, 10211. Urano, Y.; Kamiya, M.; Kanda, K.; Ueno, T.; Hirose, K.; Nagano, T. *J. Am. Chem. Soc.* **2005**, *127*, 4888.

(11) Rudolf, R.; Mongillo, M.; Rizzato, R.; Pozzan, T. *Nat. Rev.* **2003**, *4*, 579.

(12) Adam, S. R.; Kao, J. P. Y.; Grynkiewicz, G.; Minta, A.; Tsien, R. Y. *J. Am. Chem. Soc.* **1988**, *110*, 3212. Martin, M. M.; Plaza, P.; Hung, D.; Meyer, Y. H. *Chem. Phys. Lett.* **1993**, *202*, 425. Mathevet, R.; Jonusauskas, G.; Rullière, C.; Létard, J.-F.; Lapouyade, R. *J. Phys. Chem.* **1995**, *99*, 15709. Martin, M. M.; Plaza, P.; Meyer, Y. H. *Chem. Phys.* **1995**, *192*, 367. Martin, M. M.; Plaza, P.; Meyer, Y. H.; Badaoui, F.; Bourson, J.; Lefevre, J.-P.; Valeur, B. *J. Phys. Chem.* **1996**, *100*, 6879. Plaza, P.; Leray, I.; Changenet-Barret, P.; Martin, M. M.; Valeur, B. *ChemPhysChem* **2002**, *3*, 668.

(13) Xu, Z.; Xiao, Y.; Qian, X.; Cui, J.; Cui, D. *Org. Lett.* **2006**, *7*, 889.

(14) Li, Y. Q.; Bricks, J. L.; Resch-Genger, U.; Weigel, W.; Rettig, W. Manuscript in preparation.

(15) Goodall, W.; Williams, J. A. G. *Chem. Commun.* **2001**, 2514. Bricks, J. L.; Slominskii, J. L.; Kudinova, M. A.; Tolmachev, A. I.; Rurack, K.; Resch-Genger, U.; Rettig, W. *J. Photochem. Photobiol., A* **2000**, *132*, 193.

(16) Wen, Z.-C.; Yang, R.; He, H.; Jiang, Y.-B. *Chem. Commun.* **2006**, 106.

(17) For example, see: Bourson, J.; Pouget, J.; Valeur, B. *J. Phys. Chem. A* **1993**, *97*, 4552. Leray, I.; Habib-Jiwan, J.-L.; Branger, C.; Soumillion, J.-Ph.; Valeur, B. *J. Photochem. Photobiol., A* **2000**, *132*, 163.

(18) Malval, J.-P.; Lapouyade, R. *Chem. Commun.* **2000**, 289. Delmond, S.; Letard, J.-F.; Lapouyade, R.; Mathevet, R.; Jonusauskas, G.; Rullière, C. *New J. Chem.* **1996**, *20*, 861. Costero, A. M.; Sanchis, J.; Gil, S.; Sanz, V.; Williams, J. A. G. *J. Mater. Res.* **2005**, *15*, 2850.

(19) Resch-Genger, U.; Li, Y. Q.; Bricks, J. L.; Spieles, M.; Rettig, W. *J. Fluoresc.* **2006**, *16*, 337.

(20) Fery-Forgues, S.; Le Bris, M. T.; Guette, J.-P.; Valeur, B. *J. Phys. Chem.* **1988**, *92*, 6233. Fery-Forgues, S.; Le Bris, M. T.; Mialocq, J.-C.; Pouget, J.; Rettig, W.; Valeur, B. *J. Phys. Chem.* **1992**, *96*, 701. Rurack, K.; Rettig, W.; Resch-Genger, U. *Chem. Commun.* **2000**, 407. Marcotte, N.; Plaza, P.; Lavabre, D.; Fery-Forgues; S.; Martin; M. M. *J. Phys. Chem. A* **2003**, *107*, 2394. Marcotte, N.; Fery-Forgues, S.; Lavabre, D.; Marguet, S.; Pivarenko, V. G. *J. Phys. Chem. A* **1999**, *103*, 3163.

(21) Rurack, K.; Koval'chuck, A.; Bricks, J. L. *J. Am. Chem. Soc.* **2001**, *123*, 6205.

(22) Kim, S. H.; Kim, J. S.; Park, S. M.; Chang, S.-K. *Org. Lett.* **2006**, *8*, 371. Kirchner, M. F.; Weissleder, R.; Josephson, L. *Bioconjugate Chem.* **2004**, *15*, 242.

(23) Examples are: Fages, F.; Desvergne, J.-P.; Bouas-Laurent, H.; Marsau, P.; Lehn, J.-M.; Kotzyba-Hibert, F.; Albrecht-Gary, A.-M.; Al-Joubbeh, M. *J. Am. Chem. Soc.* **1989**, *111*, 8672. Cho, H. K.; Lee, D. H.; Hong, J.-L. *Chem. Commun.* **2005**, 1690. Desvergne, J.-P.; Bouas-Laurent, H.; Perez-Inestrosa, E.; Marsau, P.; Cotrait, M. *Coord. Chem. Rev.* **1999**, *185*−*186*, 357. Suzuki, Y.; Morozumi, T.; Nakamura, H.; Shimomura, M.; Hayashita, T.; Bartsh, R. A. *J. Phys. Chem. B* **1998**, *102*, 7910. Bencini, A.; Bianchi, A.; Lodeiro, C.; Casotti, A.; Parola, J.; Pina, F.; de Melo, J. S.; Valtancoli, V. *Chem. Commun.* **2000**, 1639. Yang, J.-S.; Lin, C.-S.; Hwang, C.-Y. *Org. Lett.* **2001**, *3*, 889. Liu, Y.; Duan, Y.; Zhang, H.-Y.; Jiang, X.-L.; Han, J.-R. *J. Org. Chem.* **2005**, *70*, 1450. Sankaran, N. B.; Nishizawa, S.; Watanabe, M.; Uchida, T.; Teramae, N. *J. Mater. Res.* **2005**, *15*, 2755. Hennrich, G.; Walther, W.; Resch-Genger, U.; Sonnenschein, H. *Inorg. Chem.* **2001**, *40*, 641. Yang, J.-S.; Lin, C.-S.; Hwang, C.-Y. *Org. Lett.* **2001**, *3*, 889.

(24) Cheng, C. J.; Jaworski, J.; Nolan, E. M.; Sheng, M.; Lippard, S. J. *Proc. Natl. Acad. Sci. U.S.A.* **2004**, *101*, 1129.

(25) Deo, S.; Godwin, H. A. *J. Am. Chem. Soc.* **2000**, *122*, 174.
(26) Ros-Lis, J. V.; Marcos, D.; Martinez-Manez, R.; Rurack, K.; Soto, V. *Angew. Chem., Int. Ed.* **2005**, *44*, 4405.
(27) Beer, P. D.; Gale, P. A. *Angew. Chem., Int Ed.* **2001**, *40*, 486.
(28) *Advanced Concepts in Fluorescence Sensing, Part B: Macromolecular Sensing*; Geddes, C. D., Lakowicz, J. R., Eds.; Topics in Fluorescence Spectroscopy 10; Plenum Press: New York, 2005.
(29) Examples are: de Silva, A. P.; Gunaratne, H. Q. N.; McCoy, C. P. *J. Am. Chem. Soc.* **1997**, *119*, 7891. Ji, H.-F.; Dabestani, R.; Brown, G. M. *J. Am. Chem. Soc.* **2000**, *122*, 9306. Iwata, S.; Tanaka, K. *J. Chem. Soc., Chem. Commun.* **1995**, 1491. de Silva, A. P.; McClenaghan, N. D. *Chem.—*Eur. J. **2004**, *10*, 574. Fedorova, O. A.; Fedorov, Y. V.; Andrjukhina, E. N.; Gromov, S. P.; Alfimov, M. V. *Pure Appl. Chem.* **2003**, *75*, 1077. Koskela, S. J. M.; Fyles, T. M.; James, T. D. *Chem. Commun.* **2005**, 945. Xu, X.; Xu, H.; Ji, H.-F. *Chem. Commun.* **2001**, 2092. de Silva, S. A.; Amorelli, B.; Isidor, D. C.; Loo, K. C.; Crooker, K. E.; Pena, Y. E. *Chem. Commun.* **2002**, 1360.
(30) Resch-Genger, U.; Hennrich, G. Redox-switchable Fluorescent Sensors. In *Advanced Concepts in Fluorescence Sensing, Part B: Macromolecular Sensing*; Geddes, C. D., Lakowicz, J. R., Eds.; Topics in Fluorescence Spectroscopy 10; Plenum Press: New York, 2005; and references therein.
(31) de Silva, A. P.; Fox, D. B.; Moody, T. S.; Weir, S. M. *Pure Appl. Chem.* **2001**, *73*, 503.
(32) Ushakov, E. N.; Nazarov, V. B.; Fedorova, O. A.; Gromov, S. P.; Chebun'kova, A. V.; Alfimov, M. V.; Barigelletti, F. *J. Phys. Org. Chem.* **2003**, *16*, 306.
(33) Brumbaugh, J.; Schleifenbaum, A.; Gasch, A.; Sattler, M.; Schultz, C. *J. Am. Chem. Soc.* **2006**, *128*, 24.
(34) de Silva, A. P.; Dixon, I. M.; Gunaratne, H. Q. N; Gunnlaugsson, T.; Maxwell, P. R. S.; Rice, T. E. *J. Am. Chem. Soc.* **1999**, *121*, 1393. Bag, B.; Bharadwaj, P. K. *Chem. Commun.* **2005**, 513.
(35) de Silva, A. P.; McClenaghan, N. D. *J. Am. Chem. Soc.* **2000**, *122*, 3965.
(36) Rurack, K.; Bricks, J. L.; Schulz, B.; Maus, M.; Reck, G.; Resch-Genger, U. *J. Phys. Chem. A* **2000**, *104*, 6171.
(37) Wilson, J. N.; Bunz, U. H. F. *J. Am. Chem. Soc.* **2005**, *127*, 4124.
(38) Resch-Genger, U.; Li, Y. Q.; Bricks, J. L.; Kharlanov, V.; Rettig, W. *J. Phys. Chem A* **2006**, *110*, 10956.
(39) Fabbrizzi, L.; Poggi, A. *Chem. Soc. Rev.* **1995**, *24*, 197.
(40) Cargill Thompson, A. M. W. *Coord. Chem. Rev.* **1997**, *160*, 1. Lohmeijer, B. G. G.; Schubert, U. S. *Macromol. Chem. Phys.* **2003**, *204*, 1072. Newkome, G. R.; Yoo, K. S.; Moorefield, C. N. *Chem. Commun.* **2002**, 2164. Berthet, J. C.; Riviere, C.; Miquel, Y. *Eur. J. Inorg. Chem.* **2002**, 1439. Holland, J. M.; Liu, X. M.; Zhao, J. P. *J. Chem. Soc., Dalton. Trans.* **2000**, 3316. Janini, T. E.; Fattore, J. L.; Mohler, D. L. *J. Organomet. Chem.* **1999**, *578*, 260. Mürner, H.-R.; Chassat, E.; Thummel, R. P.; Bünzli, J.-C. G. *J. Chem Soc., Dalton Trans.* **2000**, 2809. Hofmeier, H.; Schubert, U. S. *Chem. Soc. Rev.* **2004**, *33*, 373.
(41) Machado, V. G.;. Baxter, P. N. W.; Lehn, J.-M. *J. Braz. Chem. Soc.* **2000**, *12*, 431. Ballardini, V.; Balzani,V.; Clemente-Leon, M. *J. Am. Chem. Soc.* **2002**, *124*, 12786. Laine, P.; Bedioui, F.; Ochsenbein, P.; Marvaud, V.; Bonin, M.; Amouyal, E. *J. Am. Chem. Soc.* **2002**, *124*, 1364. Flamini, L.; Barigelletti, F.; Armaroli, N.; Collin, J. P.; Dixon, I. M.; Sauvage, J. P.; Williams, J. A. G. *Coord. Chem. Rev.* **1999**, *192*, 671.
(42) See, for example: Padilla-Tosta, M. E.; Lloris, J. M.; Martinez-Manez, R. *Eur. J. Inorg. Chem.* **2001**, 1475. Ziessel, R. *J. Inclusion Phenom. Macrocyclic Chem.* **1999**, *35*, 369. Whittle, B.; Batten, S. R.; Jeffery, J. C.; Rees, L. H.; Ward, M. D. *J. Chem. Soc., Dalton Trans.* **1996**, 4249. Al Shihadeh, Y.; Benito, A.; Lloris, J. M.; Martinez-Manez, R.; Soto, J. *Transition Met. Chem.* **2002**, *27*, 307. Barigletti, F.; Flamigni, L.; Calogero, G.; Hammarström, L.; Sauvage, J. P.; Collin, J.-P. *Chem. Commun.* **1998**, 2333. Goodall, W.; Williams, J. A. G. *J. Chem. Soc., Dalton. Trans.* **2000**, 2893. Yam, V. W.-W.; Lee, V. W.-M., *J. Chem. Soc., Dalton. Trans.* **1997**, 3005. Licini, M.; Williams, J. A. G. *Chem. Commun.* **1999**, 1943. Che, C.-M.; Zhang, J.-L.; Lin; L.-R. *Chem. Commun.* **2002**, 2556. de Silva, A. P.; Gunaratne, H. Q. N.; Rice, T. E.; Stewart, S. *Chem. Commun.* **1997**, 1891. Tang, W.-S.; Lu, X.-X.; Wong, K. M.-C.; Yam, V. W.-W. *J. Mater. Chem.* **2005**, *15*, 2714.
(43) Buschel, M.; Helldobler, M.; Daub, J. *Chem. Commun.* **2002**, 1338.
(44) Constable, E. C.; Smith, D. R. *Supramol. Chem.* **1994**, *4*, 5. Goodall, W.; Williams, J. A. G. *Chem. Commun.* **2001**, 2514. Albano, G.; Balzani, V.; Constable, E. C.; Maestri, M.; Smith, D. R. *Inorg. Chim. Acta* **1998**, *277*, 225.
(45) Maus, M.; Rettig, W.; Bonafoux, D.; Lapouyade, R. *J. Phys. Chem. A* **1999**, *103*, 3388.
(46) Lahmani, F.; Breheret, E.; Zehnacker-Rentien, A.; Amatore, C.; Jutand, A. *J. Photochem. Photobiol., A* **1993**, *70*, 39.
(47) Herbich, J.; Waluk, J. *Chem Phys.* **1994**, *188*, 247.
(48) Chou, P. T.; Chang, C. P.; Clements, J. H.; Meng-Shin, K. *J. Fluoresc.* **1995**, *5*, 369.
(49) Ephardt, H.; Fromherz, P. *J. Phys. Chem.* **1991**, *95*, 6792. Fromherz, P.; Heilemann, A. *J. Phys. Chem.* **1992**, *96*, 6864. Röcker, C.; Heilemann, A.; Fromherz, P. *J. Phys. Chem.* **1996**, *100*, 12172.
(50) Maus, M.; Rettig, W. *J. Inf. Rec.* **1998**, *24*, 461. Maus, M.; Rettig, W. *Chem. Phys.* **1997**, *218*, 151. Maus, M.; Rettig, W.; Lapouyade, R. *J. Inf. Rec.* **1996**, *22*, 451.
(51) TICT: twisted intramolecular charge transfer.
(52) For a recent review, see: Grabowski, Z. R.; Rotkiewicz, K.; Rettig, W. *Chem. Rev.* **2003**, *103*, 3899.
(53) *Gmelins Handbuch der Anorganischen Chemie*, 8th ed.; VCH: Berlin, 1927.
(54) Resch-Genger, U.; Pfeifer, D.; Monte, C.; Pilz, W.; Hoffmann, A.; Spieles, M.; Rurack, K.; Hollandt, J.; Taubert, D.; Schönenberger, B.; Nording, P. *J. Fluoresc.* **2005**, *15*, 315.
(55) Pfeifer, D.; Hoffmann, K.; Hoffmann, A.; Monte, C.; Resch-Genger, U. *J. Fluoresc.* **2006**, *16*, 581.
(56) *Principles of Fluorescence Spectroscopy*; 2nd ed.; Lakowicz, J. R., Ed.; Kluwer Academic/Plenum Press: New York, 1999.
(57) Demas, J. N. *Optical Radiation Measurements*; Mielenz, K. D., Ed.; Academic Press: New York, 1982; Vol. 3, p 195.
(58) Drexhage, K. H. *J. Res. Natl. Bur. Stand. (U.S.)* **1976**, *80A*, 421.
(59) *Time-Correlated Single-Photon Counting*; Connor, D. V., Phillips, D., Eds.; Academic Press: London, 1984.
(60) Weigel, W.; Rettig, W.; Dekhtyar, M.; Modrakowski, C.; Beinhoff, M.; Schlüter, A. D. *J. Phys. Chem. A* **2003**, *107*, 5941.
(61) Globals Unlimited. Laboratory of Fluorescence Dynamics at the University of Illinois, 1992.
(62) Moya, S. A.; Pastene, R.; Le Bozec, H.; Baricelli, P. J.; Pardey, A. J.; Gimeno, J. *Inorg. Chim. Acta* **2001**, *312*, 7.
(63) Spahni,W.; Calzagerri, G. *Helv. Chim. Acta* **1984**, *67*, 450.
(64) Mutai, T.; Cheon, J.-D.; Arita, S.; Araki, K. *J. Chem. Soc., Perkin Trans. 2* **2001**, 1045.
(65) Gleb, U.; Priimov, M.; Peter, H.; Lothar, M.; Andre, E. *Inorg. React. Mech.* **2001**, *3*, 1.
(66) Vosburgh, W. C.; Cooper, G. R. *J. Am. Chem. Soc.* **1941**, *63*, 437.
(67) Grynkiewicz, G.; Poenie, M.; Tsien, R. Y. *J. Biol. Chem.* **1985**, *260*, 3440. Maruyama, S.; Kikuchi, K.; Hirano, T.;. Urano, Y.; Nagano, T. *J. Am. Chem. Soc.* **2002**, *124*, 10650.
(68) Marcotte, N.; Plaza, P.; Lavabre, D.; Fery-Forgues, S.; Martin, M. M. *J. Phys. Chem. A* **2003**, *107*, 2394 and references therein.
(69) Maus, M.; Rurack, K. *New J. Chem.* **2000**, *24*, 677.
(70) Rettig, W.; Kharlanov, V.; Maus, M. *Chem. Phys. Lett.* **2000**, *318*, 173. Kharlanov, V. A.; Abraham, W.; Rettig, W. *J. Photochem. Photobiol., A* **2001**, *143*, 109.
(71) Siebrand, W. *J. Chem. Phys.* **1966**, *44*, 4055.
(72) The energy gap law predicts an exponential increase of k_{isc} or k_{nr} with decreasing difference between S_1 and the nearest lower lying state.
(73) The explanation of an anti-energy gap rule behavior relies on radiative and nonradiative rate constants deduced from measured fluorescence quantum yields and fluorescence lifetimes, thereby assuming a yield of 1 for the formation of the CT state. This is fulfillled for the cation complexes of bpb-R, where no LE emission is observed. Accordingly, no attempts have been made to, e.g., determine radiative rate constants from absorption spectra to discriminate emission from the initially excited state or from a transient state that could not be detected within the limited time resolution of our setup.
(74) Sarkar, A.; Chakravorti, S. *J. Lumin.* **1995**, *63*, 143.
(75) Delmond, S.; Létard, J.-F.; Lapouyade, R. *New J. Chem.* **1996**, *20*, 851.
(76) Raymo, F. M. *Adv. Mater.* **2002**, *14*, 401.
(77) Balzani, V.; Credi, A.; Venturi, M. *ChemPhysChem* **2003**, *3*, 49.
(78) de Silva, A. P., Gunaratne, H. Q. N.; McCoy, C. P. *Nature* **1993**, *364*, 42.
(79) de Silva, A. P.; Gunaratne, H. Q. N.; McCoy, C. P. *J. Am. Chem. Soc.* **1997**, *119*, 7891.
(80) de Silva, A. P.; Dixon, I. M.; Gunaratne, H. Q. N.; Gunnlaugsson, T.; Maxwell, P. R. S.; Rice, T. E. *J. Am. Chem. Soc.* **1999**, *121*, 1393.
(81) Gunnlaugsson, T.; MacDonail, D. A.; Parker, D. *J. Am. Chem. Soc.* **2001**, *123*, 12866.
(82) de Silva, A. P.; Rupasinghe, R. A. D. D. *J. Chem. Soc., Chem. Commun.* **1985**, 1669.
(83) de Silva, A. P.; Gunnlaugsson, T.; McCoy, C. P. *J. Chem. Educ.* **1997**, *74*, 53.
(84) Loiseau, F.; Di Pietro, C.; Campagna, S.; Cavazzini, M.; Marzanni, G.; Quici, S. *J. Mater. Chem.* **2005**, *15*, 2763.
(85) Constable, E. C.; Henney, R. P. G.; Tocher, D. A. *J. Chem. Soc., Dalton Trans.* **1992**, 2467.